Impact of Inherited Foreland Relief on Retro-Foreland Basin Architecture

Benjamin Gérard, Delphine Rouby, Ritske S Huismans, Cécile Robin, Charlotte Fillon, Jean Braun

JGR Solid Earth

RESEARCH ARTICLE
10.1029/2022JB024967

Impact of Inherited Foreland Relief on Retro-Foreland Basin Architecture

Benjamin Gérard[1,2], Delphine Rouby[1], Ritske S. Huismans[3], Cécile Robin[4], Charlotte Fillon[5], and Jean Braun[6,7]

[1]GET, CNRS, IRD, UPS, Université de Toulouse, Toulouse, France, [2]Laboratoire de Planétologie et Géosciences, CNRS UMR 6112, Nantes Université/Université d'Angers/Le Mans Université, Nantes, France, [3]Department of Earth Sciences, Bergen University, Bergen, Norway, [4]CNRS, Géosciences Rennes, UMR6118, University of Rennes, Rennes, France, [5]TotalEnergies, Centre Scientifique et Technique Jean Féger, Pau Cédex, France, [6]Helmholtz Centre Potsdam, German Research Centre for Geosciences, Potsdam, Germany, [7]Institute of Geosciences, University of Potsdam, Potsdam, Germany

Key Points:

- An elevated foreland domain produces a thinner flexural basin than a low foreland as more sediment is bypassed
- A deep foreland produces a thicker flexural basin than a low foreland because of the extra load of the inherited space filling
- A deep foreland is required to preserve a significant proportion of deep marine deposits in the foreland flexural basin

Supporting Information:

Supporting Information may be found in the online version of this article.

Correspondence to:

B. Gérard,
benjamin.gerard@univ-nantes.fr

Citation:

Gérard, B., Rouby, D., Huismans, R. S., Robin, C., Fillon, C., & Braun, J. (2023). Impact of inherited foreland relief on retro-foreland basin architecture. *Journal of Geophysical Research: Solid Earth*, *128*, e2022JB024967. https://doi.org/10.1029/2022JB024967

Received 12 JUN 2022
Accepted 6 MAR 2023

Author Contributions:

Conceptualization: Benjamin Gérard, Delphine Rouby, Ritske S. Huismans, Cécile Robin, Charlotte Fillon, Jean Braun
Formal analysis: Benjamin Gérard, Delphine Rouby
Funding acquisition: Delphine Rouby, Ritske S. Huismans, Jean Braun
Investigation: Benjamin Gérard, Delphine Rouby, Ritske S. Huismans, Cécile Robin
Methodology: Benjamin Gérard
Resources: Delphine Rouby
Software: Benjamin Gérard, Jean Braun
Supervision: Delphine Rouby, Ritske S. Huismans, Cécile Robin

Abstract We use a Landscape Evolution Model including flexural isostasy to investigate the influence of inherited foreland relief on the stratigraphic evolution of the retro-foreland domain during mountain building. We show models with four different types of initial relief in the foreland domain: at sea level, elevated (+300 m), a 1 km-deep and 100 km-wide foreland basin associated with either a forebulge at sea level or elevated at +300 m. During the first 10 Myr of simulation, the landscape evolution of the foreland is significantly altered by its inherited bathymetry/topography. The impact is then smoothed out once the foreland slope has stabilized and develops a transverse drainage network. Models record a long-term shallowing-up mega-sequence driven by the increase in sediment production rate in the uplifting range and the decrease in the rate of flexural accommodation space creation in the foreland basin. The initial relief of the foreland domain alters the timing of its transition from the under-filled to the over-filled phase. An initially deep foreland basin is twice as thick as an initially elevated foreland. It records deep marine deposits while a foreland initially at sea level records thin shallow marine and an elevated foreland records continental deposits. The forebulge is buried by continental deposits in an initially elevated foreland while it is buried by marine sediments in other models. Alluvial fans at the foot of the range are more elevated in initially elevated forelands. We discuss our results of modeled stratigraphic architecture in comparison with the Pyrenean, Alpine and Andean retro-foreland basins.

Plain Language Summary Rising mountain ranges locally thicken the Earth's crust and the extra load generates lateral depressions where sediments eroded in the mountain range can be stored. This process forms foreland sedimentary basins that record the growth of the mountain range. We simulated the evolution of the landscape of a mountain range to test the impact of different initial topographies of the foreland at the foot of the mountain range: low (0 m), elevated (+300 m), and deep (−1,000 m). All models show a common evolution driven by the creation of mountain range topography and development of lateral depressions, the build-up and connection of alluvial fans at the foot of the range followed by their progressive migration away from the range. An initially elevated foreland preserves less sediment and produces an ultimately thinner sedimentary basin than low lying or deep forelands. Erosion and sedimentation processes erase any trace of inherited relief in the landscape after ∼10–13 Myr. On the other hand, the geometry of the sediment strata in the foreland basin records the initial topography: the low and deep forelands are initially covered by marine sediments while only the initially elevated forelands are initially covered by continental sediments.

1. Introduction

Foreland basins are unique records of the evolution of orogenic mountain ranges as they collect, preserve, and recycle the products of their erosion. Accommodation variations in the proximal foreland basin and in the more distal forebulge area are mainly driven by the flexural isostatic response of the lithosphere to the topographic load of the growing range (e.g., Beaumont, 1981; DeCelles & Giles, 1996; Quinlan & Beaumont, 1984). In addition, surface processes constantly alter the flexural response to the topographic and sediment loads by controlling the sediment routing systems, erosion of the range, and sediment accumulation in the foreland basin (e.g., Beaumont, 1981; DeCelles & Giles, 1996; Flemings & Jordan, 1989; Jordan & Flemings, 1991; Simpson, 2006).

Because of these couplings, the first-order stratigraphic record of foreland basins usually evolves from an "underfilled phase" frequently recording marine and coastal depositional environments to an "overfilled phase"

Validation: Benjamin Gérard, Delphine Rouby, Ritske S. Huismans, Cécile Robin, Charlotte Fillon, Jean Braun
Visualization: Benjamin Gérard
Writing – original draft: Benjamin Gérard
Writing – review & editing: Benjamin Gérard, Delphine Rouby, Ritske S. Huismans, Cécile Robin, Charlotte Fillon, Jean Braun

recording fluvial plain and alluvial fan depositional environments (sensu Catuneanu, 2004, 2017), forming a continentalization "coarsening-up" and prograding mega-sequence (e.g., Catuneanu, 2004; Clevis et al., 2004; DeCelles, 2012; DeCelles & Giles, 1996; Einsele, 1992; Jordan, 1995; Schlunegger et al., 1997; Sinclair & Allen, 1992). The shape of the basin, the duration of the phases, and the associated facies are highly dependent on parameters including the uplift rate of the mountain range, the effective elastic thickness of the lithosphere (EET) controlling the flexural isostasy, the base-level, the erosion efficiency, and the transport/sedimentation efficiency (e.g., Allen et al., 2013; Beaumont, 1981; Catuneanu, 2004; Clevis et al., 2004; DeCelles & Giles, 1996; Flemings & Jordan, 1989, 1990; Jordan & Flemings, 1991; Simpson, 2006; Sinclair et al., 1991; Tucker & van der Beek, 2013). For example, using coupled flexural isostasy and surface processes modeling, Flemings and Jordan (1989) and Sinclair et al. (1991) show that faster thrusting rates (i.e., faster range uplift) result in narrower and less filled foreland basins than slower thrusting rates. They also show that the transition from the underfilled to overfilled phase can be solely driven by more or less efficient erosion and sedimentation surface processes (e.g., lithology, precipitation or base-level).

Another parameter impacting foreland stratigraphic evolution is the inheritance from rifting before the collision. Mountain ranges often develop in previously rifted domains, as for instance in Tethyan orogenic systems such as the Pyrenees and the Alps (e.g., Beaumont et al., 2000; Desegaulx et al., 1991; Schlunegger et al., 1997; Stampfli & Hochard, 2009; Vacherat et al., 2017). Watts (1992), Stewart and Watts (1997) and Leever et al. (2006) have analyzed the impact of inheritance from a previous rifting event on the evolving EET and evolution of foreland basins. In the northern Pyrenees, Angrand et al. (2018), Desegaulx et al. (1991) and Desegaulx and Brunet (1990) showed that tectonic inheritance, and more specifically, the thermal and crustal structure has a strong impact on foreland basin geometry. Despite these studies, the effect of inherited topography or bathymetry in the proto-foreland domain on stratigraphic architecture of foreland basins have not been addressed yet. Indeed, the impact of structures inherited from rifting on orogenic deformation has been widely studied (e.g., Erdos et al., 2014; Wolf et al., 2021), but the implications for the stratigraphic architecture of foreland basins remains to be constrained. Remnants of a previous extensional phase in the relief of an initial foreland domain can potentially significantly impact its capacity to trap sediments produced in the mountain range and in doing so, the shape of the foreland basin, the duration of the underfilled/overfilled phases, as well as the associated paleo-environments. The aim of this work is to explore this effect and compare its magnitude to other controlling parameters such as mountain range uplift rate, EET of the foreland lithosphere, and erosion/transport/sedimentation efficiency.

To do this, we use a Landscape Evolution Model (LEM) taking into account flexural isostasy and both marine and continental sedimentary processes (FastScape S2S; Yuan, Braun, Guerit, Rouby, & Cordonnier, 2019; Yuan, Braun, Guerit, Simon, et al., 2019). The LEM allows assessing, in 3D, the relationships between flexural isostasy, landscape evolution and stratigraphic architecture of the foreland basin (Figure 1). We focus on the stratigraphic architecture of the retro-wedge foredeep, between the frontal tip of the orogenic wedge and the forebulge (DeCelles & Giles, 1996). This allows us to approximate the syn-orogenic evolution using only vertical motion (uplift and flexural isostasy) as retro-wedge systems of small to intermediate size orogens are less affected by horizontal advection related to thrusting (Grool et al., 2018; Naylor & Sinclair, 2008; Willett et al., 1993; Wolf et al., 2021). We compare our simple cylindrical setups and generic approach to the Pyrenean, Andean, and Alpine retro-foreland systems, in order to discuss the potential effect of inherited topography and/or bathymetry on the evolution of these foreland basins.

2. Materials and Methods

We use the numerical LEM FastScape (Bovy, 2021; Braun & Willett, 2013; Guerit et al., 2019; Yuan, Braun, Guerit, Rouby, & Cordonnier, 2019; Yuan, Braun, Guerit, Simon, et al., 2019). The model simulates the evolution of a fluvial landscape including sediment production, transport and continental deposition, marine deposition, as well as the flexural isostatic response of the lithosphere to associated loading and unloading (Braun & Willett, 2013; Guerit et al., 2019; Yuan, Braun, Guerit, Rouby, & Cordonnier, 2019; Yuan, Braun, Guerit, Simon, et al., 2019; see details in Text S1 in Supporting Information S1).

Our model setup provides a simplified representation of orogenic retro-wedge systems. It consists of a half mountain range (150 × 400 km) uplifting at a constant rate (0.5 mm/yr; Figure 1; Table 1) but not migrating for 25 Myr. Eroded material produced in the uplifted area is transported to a foreland domain (350 × 400 km) and, beyond,

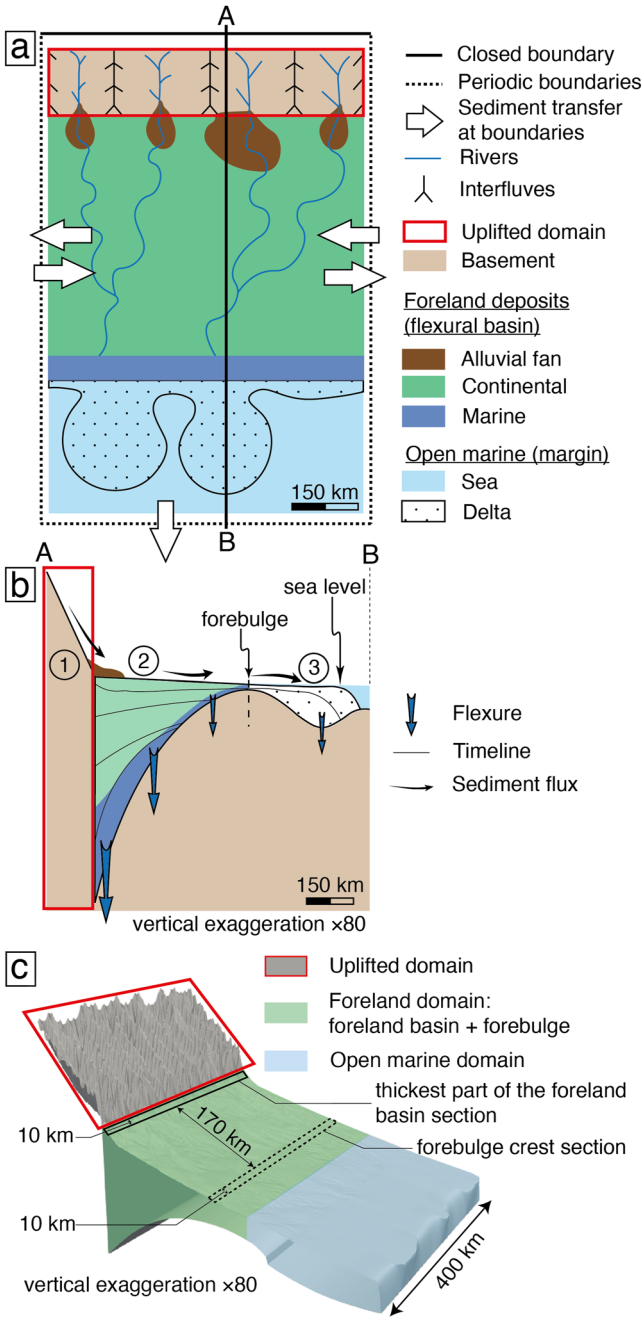

Figure 1. (a) Top view of the model setup and associated landscape domains. Lateral periodic boundaries imply that sediments exiting the model on one side re-enter it on the opposite side. (b) Cross section (location in a) with (1) the uplifted domain, (2) the foreland domain (foreland basin and forebulge) and (3) the open marine domain. (c) Perspective view of the model showing the location of the thickest foredeep and forebulge crest sections.

to a distal open marine domain (200 × 400 km; Figure 1; Table 1). The foreland domain includes the foreland basin and the forebulge controlled by flexural isostasy (Figure 1) which does not migrate. The distal open marine domain is a boundary condition inspired by the Pyrenean system (Bernard & Sinclair, 2022; Ortiz et al., 2020) although we did not simulate the non-cylindrical configuration of the natural case. The distal marine domain has been included to avoid border effects which would affect the dynamics of continental deposition in our models. This distal domain is included, but not discussed. We present four models with varying initial topography and bathymetry in the foreland (Figure 2): Reference model M1 with a foreland domain initially at sea level (Figure 2a); Model M2 with a foreland domain elevated at +300 m (Figure 2b); Model M3 with a 100 km-wide and 1,000 m-deep water filled basin in the foreland domain and a 250 km-wide forebulge area at sea level (Figure 2c); Model M4 with a 100 km-wide and 1,000-m deep water filled basin in the foreland domain and an elevated foreland area 300 m above sea level (Figure 2d). Model M1 is a reference model to allow comparisons.

The initial bathymetry at the foot of the range in M3 and M4 represents pre-existing rift related topography that can be encountered in natural orogenic systems such as the Pyrenees (e.g., Desegaulx et al., 1991). The associated elevated forebulge is consistent with the paleogeographic reconstruction of the Northern Pyrenean system ~55 Myr ago by Vacherat et al. (2017). The initially elevated foreland domain in models M2 and M4 represents stable Phanerozoic continents that have an average elevation of ~400 ± 400 m (e.g., Theunissen et al., 2022). Model duration (25 Myr), is consistent with the time span between the main phase of Pyrenean topography emergence (~55 Myr) and the syn- to post-orogenic transition ~27 Myr (e.g., Curry et al., 2019; Vacherat et al., 2017). Although inspired by the Pyrenees, this simple configuration can also be compared to other orogenic systems such as the Alpes or the Andes to discuss their retro-forelands sedimentary dynamics. To initiate rivers grading toward the foreland domain, we impose a gentle initial tilt of the uplifted domain ($\alpha = 0.076°$; Figure 2).

In the four models, we use parameter values generally admitted in the literature (Table 1). A constant and homogenous precipitation rate $P = 0.5$ m/yr, effective elastic thickness EET = 15 km (Garcia-Castellanos & Cloetingh, 2012), fluvial erodibility $K_f = 2.5 \times 10^{-5}$ m$^{0.2}$/yr (Whipple & Tucker, 1999), hillslope diffusion $K_h = 1.0 \times 10^{-2}$ m^2/yr (Armitage et al., 2013; Densmore et al., 2007), continental deposition coefficient $G = 0.4$ (Davy & Lague, 2009; Guerit et al., 2019), and marine diffusion coefficient $K_d = 2.0 \times 10^2$ m^2/yr (Jordan & Flemings, 1991; Rouby et al., 2013; Yuan, Braun, Guerit, Simon, et al., 2019; Table 1). For marine diffusion, we use values representative of a silty grain-size (Rouby et al., 2013; Simon et al., 2022). Sediment compaction is not included.

For the analysis of the stratigraphic architecture, we use the definition of Catuneanu (2004, 2017) and Sinclair and Allen (1992) of the underfilled, filled, and overfilled stages in the evolution of the foreland basin in which depositional processes are dominated by deep marine, shallow marine, or fluvial sedimentation, respectively.

3. Results

3.1. Reference Model M1

In reference model M1, the mountain range grows gradually to an average topography of 1.7 km elevation at 25 Myr (Figures 3, 4a, and 5a). The basement of the flexural foreland basin subsides progressively under the increasing

Table 1
Common Parameters of the Models

Parameter	Value	Unit
Size of the model domain	400×700	km
Size of the cell (d_x, d_y)	1,000	m
Time step (d_t)	1,000	yr
Total duration	25×10^6	yr
Uplift rate (U)	0.5	mm/yr
Precipitation rate (P)—homogeneous and constant	0.5	m/yr
Effective Elastic thickness (EET)	15[a]	km
Erodibility (K_f)	2.5×10^{-5}[b]	$m^{0.2}$/yr
Hillslope diffusion coefficient (K_h)	1.0×10^{-2}[c,d]	m^2/yr
Continental deposition coefficient (G)	0.4[e,f]	–
Erosion law coefficients (m, n)	0.4[g], 1[h]	–
Sea level elevation	0	m
Marine diffusion coefficient (K_d)	2.0×10^2[i,j,k,l]	m^2/yr

Note. The erodibility value (K_f) was chosen to reach a mean mountain range elevation of ~1.7 km after 25 Myr.

[a]Parameters from Garcia-Castellanos and Cloetingh (2012). [b]Parameters from Whipple and Tucker (1999). [c]Parameters from Densmore et al. (2007). [d]Parameters from Armitage et al. (2013). [e]Parameters from Davy and Lague (2009). [f]Parameters from Guerit et al. (2019). [g]Parameters from Stock and Montgomery (1999). [h]Parameters from Braun and Willett (2013). [i]Parameters from Jordan and Flemings (1991). [j]Parameters from Rouby et al. (2013). [k]Parameters from Yuan, Braun, Guerit, Simon, et al. (2019). [l]Parameters from Simon et al. (2022).

load of the mountain range topography and of the sediments to a maximum depth of 2.6 km (Figures 3 and 5c). Initially, the depositional environments are shallow marine and the forebulge is partly submerged (Figures 3a and 4a; Movie S1). Part of the sediments produced by erosion of the mountain belt fills the flexural foreland basin while the remainder is exported to the marine domain (Figures 3a and 4a). After a 3.7 Myr, alluvial deposits and initially isolated and progressively coalescing alluvial fans (i.e., sediment deposited at a slope >0.4°; Bull, 1964; Milana & Ruzycki, 1999) form at the foot of the mountain range (Figures 3b and 4a). This transition is slightly diachronous laterally, due to relief heterogeneities depending on the local relief of the mountain range and previously deposited sediments (Movie S1). Afterward, the shoreline and the continental deposits progressively migrate from the foot of the mountain range toward the forebulge as the foreland basin evolves toward marine to continental environments (continentalization; Figures 3b and 4a). At the same time, alluvial fans at the foot of the range migrate away and toward the mountain range. These oscillations are driven by the competition between local erosion and the space available for deposition, which is controlled by the deposition of previous fans, local relief, and individual drainage dynamics (Movie S1). These short-term oscillations do not alter the general migration of continental deposits across the foreland basin. At 15 Myr, continental deposits reach the forebulge and at 25 Myr, the foreland basin and the forebulge are entirely continentalized (Figures 3c, 3d, and 4a; Movie S1).

3.2. Models M2 to M4 With Inherited Topography/Bathymetry in the Foreland Domain

Models with inherited topography and/or bathymetry in the foreland domain (M2 to M4) follow a first order trend common with the reference model M1: initial building of the mountain range topography, development of the flexural foreland basin and forebulge, formation and coalescence of alluvial fans at the foot of the mountain range, and progressive migration of continental deposits across of the foreland domain (Figure 4, and Figures S1–S3 in Supporting Information S1). Inherited topography and/or bathymetry in the foreland domain do nevertheless have a significant impact on the timing and depositional environments of this trend (Figure 4, and Figures S1–S3 in Supporting Information S1).

The initially elevated foreland domain of model M2 (+300 m; Figure 2b) records only continental sediments (alluvial deposits and fans), allows for less material to be trapped at the foot of the range and is rapidly incised by a regressive erosion that connects the mountain range to the open marine domain (within 1 Myr; Figure 4b and Figure S1 in Supporting Information S1; Movie S2). These river networks, not only export sediments produced in the mountain range, but also remobilize sediments previously stored in the foreland basin. In contrast with the reference model M1, this open marine domain is entirely filled and continentalized after 25 Myr suggesting that more sediments were exported (Figure 4b and Figure S1 in Supporting Information S1).

In model M3, sediments produced in the mountain range are trapped in the initially water filled basin at the foot of the range (1,000 m deep; Figure 2c) in deep marine depositional environments during the first 7 Myr (Figure 4c and Figure S2 in Supporting Information S1; Movie S3). The foreland basin progressively fills up to shallow marine deposits and the forebulge is progressively submerged and buried by shallow marine deposits. First fluvial deposits emplaced at the foot of the range at 3 Myr, followed by alluvial fans that start accumulating by 6 Myr (Figure 4c and Figure S2 in Supporting Information S1; Movie S3). The shoreline and continental deposits migrate across the foreland to reach the forebulge that is starting to be buried by continental sediments by 13 Myr (Figure 4c and Figure S2 in Supporting Information S1; Movie S3).

In model M4, combining an initially deep water filled basin and an elevated foreland domain, the foreland also traps deep marine sediments, and the initially elevated foreland is rapidly incised (within 1 Myr; Figure 4d and Figure S3 in Supporting Information S1; Movie S4). Sediments produced by erosion of the forebulge area contribute to the filling of the foreland basin in addition to the sediments produced by erosion of the range. Similar to model M2, once the initial bathymetry is filled to shallow marine depositional environments and then

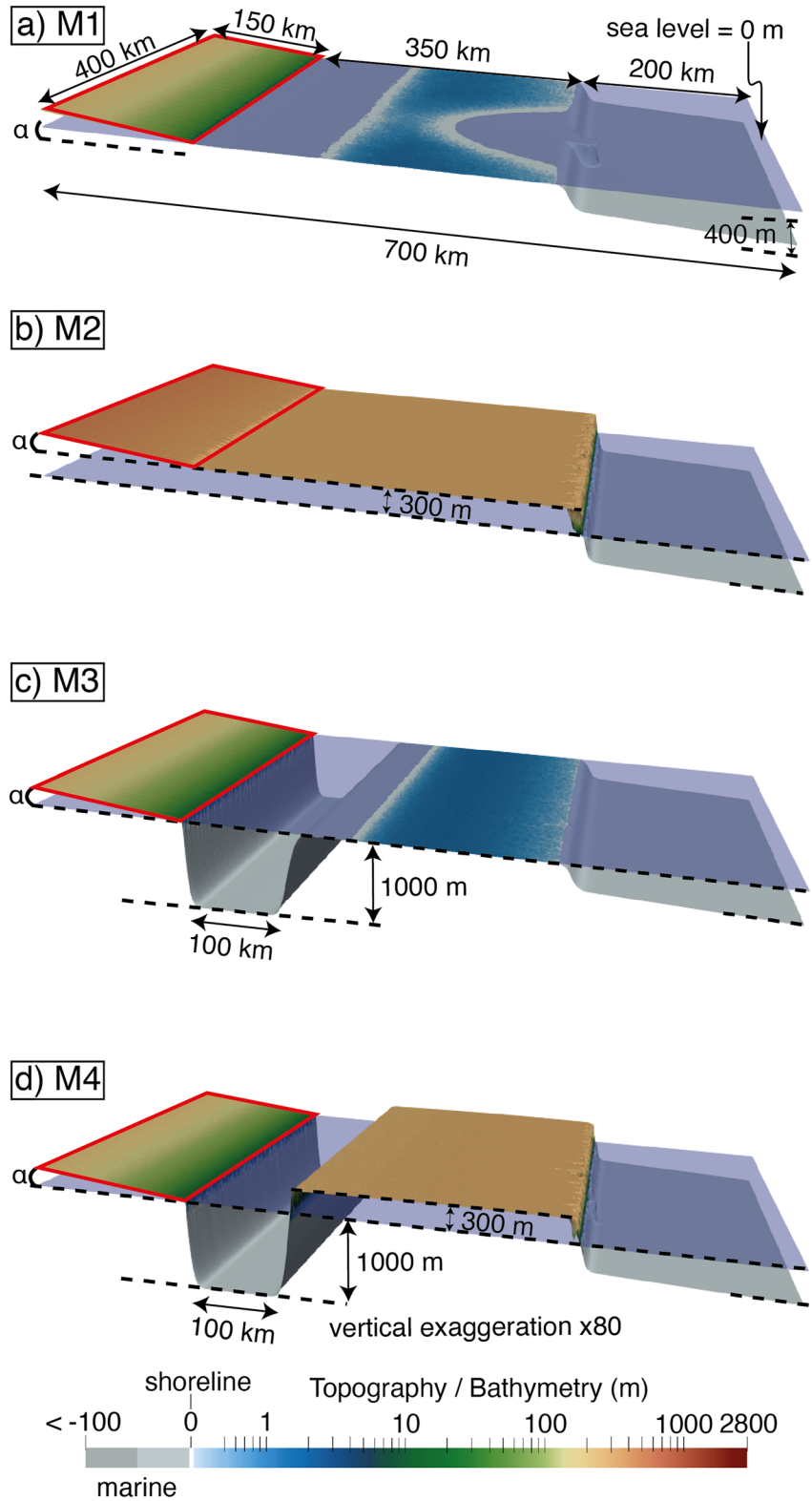

Figure 2. Setup for models M1–M4. (a) M1, foreland domain at sea level. (b) M2, elevated foreland domain (+300 m). (c) M3, the foreland domain is composed of a water filled basin (100 km wide and 1,000 m deep) and forebulge at sea level (250 km wide). (d) M4, the foreland domain is composed of a water filled basin (100 km wide and 1,000 m deep) and an elevated forebulge area (250 km wide and elevated at +300 m). Initial slopes of the uplifted orogenic domains (red box) are identical ($\alpha = 0.076°$).

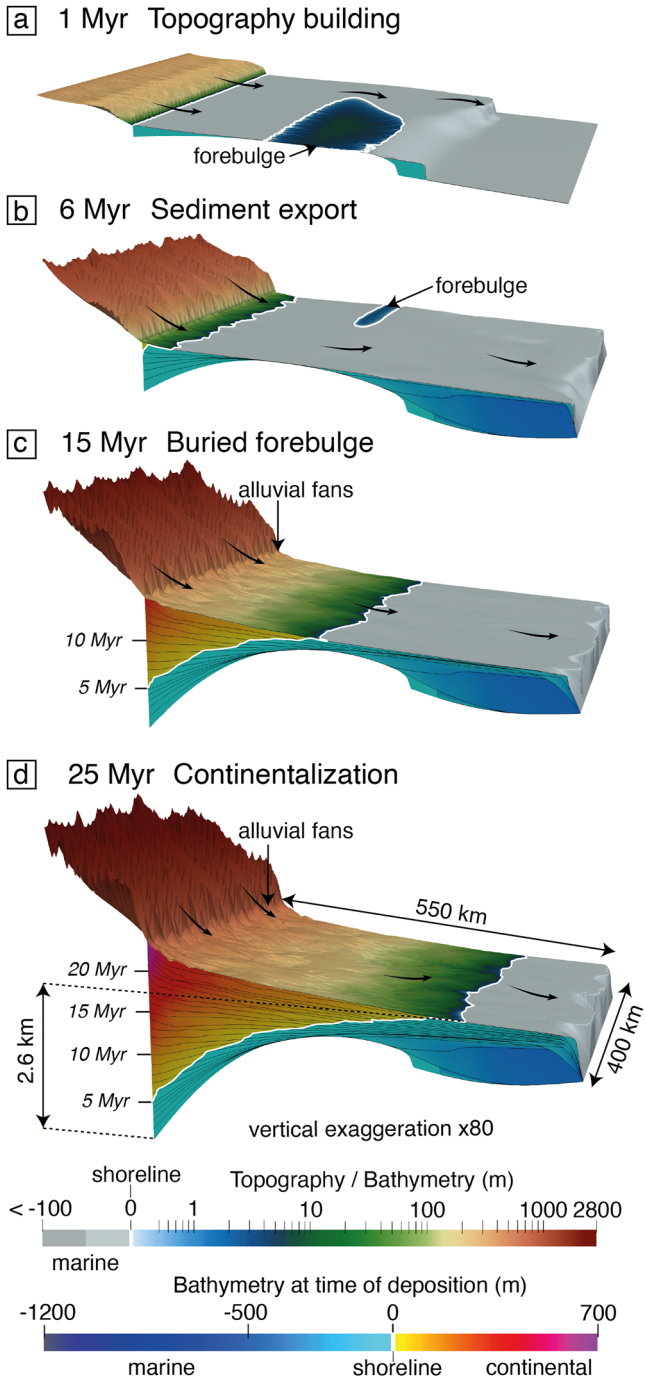

Figure 3. Evolution of model M1 at (a) 1 Myr; (b) 6 Myr, (c) 15 Myr and (d) 25 Myr. The surface of the model is colored according to the topography and bathymetry. The section of the model is colored according to the depositional bathymetry. Black arrows represent sediment transport directions.

continentalized (~4.6 Myr), the whole foreland domain is incised by regressive erosion remobilizing previously deposited sediments.

3.3. General Characteristics of Mountain Range and Foreland Basin Evolution

We evaluate the evolution of mean elevation, mean erosion rate, foreland basin depth, and sediment volume in the models (Figure 5). The evolution of the mean elevation of the uplifted domain is very similar in the four models and shows a progressive build-up to ~1.7 km after 25 Myr, without reaching steady state (Figure 5a). Associated mean erosion rates in the mountain range follow a similar overall increase to 3.5–4.0 $\times$ 10^{-4} m/yr at 25 Myr (Figure 5b). During this increase however, all models undergo abrupt drops in mean erosion rates (ca. two-fold decrease; Figure 5b). The timing of the drops in erosion rate varies from one model to the other (5.2, 4.9, and 3 Myr in Models 1, 2, and 3 respectively). Model M4 shows a more complex behavior with a first drop at 4.6 Myr and a second one at 11.9 Myr associated with a few oscillations. After the drops, all models return to a trend of increasing mean erosion rates over time (Figure 5b). This particular behavior is further discussed below. Figure S4 in Supporting Information S1 provides a top view of the erosion and deposition rates above sea level through time.

The maximum basement depths of the foreland basins of M1–M4 exhibit similar deepening trends but reach different final depths at 25 Myr (e.g., 2.6 km for M1, 2.3 km for M2, 3.6 km for M3 and 3.4 km for M4; Figure 5c). The total volume of sediments produced in the mountain range is similar in the four models (4–4.5 $\times$ 10^{14} m^3). However, the volume of sediment accumulated in the foreland basin is quite different between the models (1.30 $\times$ 10^{14}, 0.95 $\times$ 10^{14}, 2.20 $\times$ 10^{14} and 1.80 $\times$ 10^{14} m^3 for M1, M2, M3, and M4 respectively; Figure 5d). This is mirrored by different proportions of sediments exported to the open marine domain (Figure 5d).

Models M1–M4 are based on identical uplift rates of the mountain range, erodibility, and EET. To assess the impact of the initial bathymetry/topography of the foreland in comparison to one of these parameters, we also performed a sensitivity analysis of model M1 to varying uplift rate, erodibility, and EET. Supplementary model SM1 shows that increasing uplift rates (0.1–1 mm/yr) increases the mean topography of the mountain range (100–1,970 m respectively), the topographic load and the flexural isostatic response of the foreland and ultimately the thickness the foreland basin (maximum depth from 0 to 2,500 m respectively; Figure S9 and Table S1 in Supporting Information S1). Supplementary model SM4 shows that increasing erodibility (0.5–9 $\times$ 10^{-5} $m^{0.2}$/yr), decreases the mountain range mean topography (2,620–360 m respectively) and the associated flexure in the foreland basin (maximum depth from 3,850 to 450 m respectively; Figure S10 and Table S1 in Supporting Information S1). Finally, supplementary model SM5 shows that increasing the EET (5–25 km), decreases the amplitude of the foreland basin flexure, and the thickness of the foreland basin infill (maximum thickness from 3,850 to 450 m respectively; Figure S11 and Table S1 in Supporting Information S1). This analysis shows that the impact of the initial bathymetry/topography of the foreland geometry is as significant as that of uplift rate, erodibility, and EET.

3.4. Foreland Basin Stratigraphic Architecture

For each model, we show the stratigraphic architecture of the foreland basin along a cross-section as well as the corresponding Wheeler diagram of the depositional bathymetry/elevation through time (Figure 6; Sections location

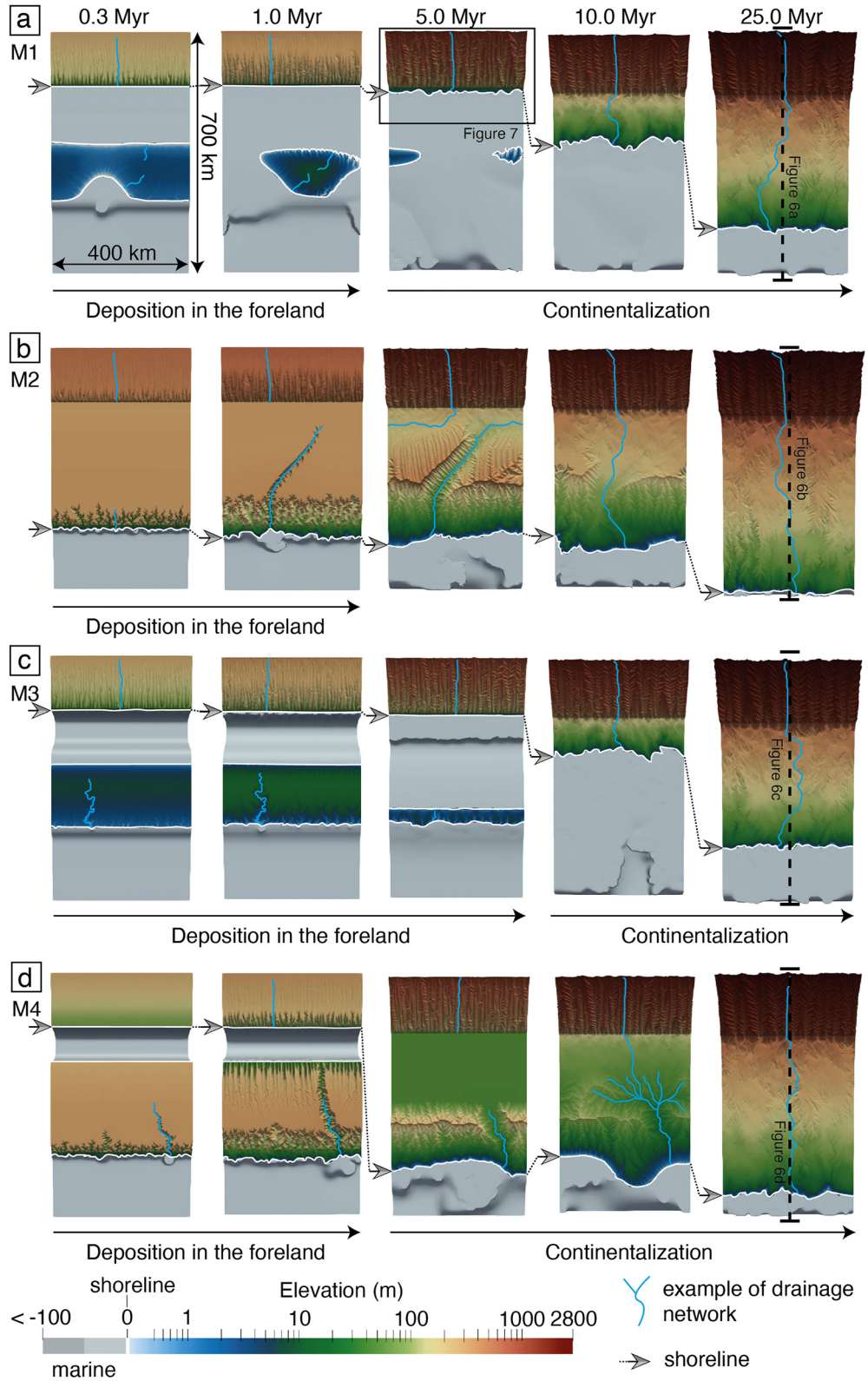

Figure 4. Top view of the topography of models (a) M1, (b) M2, (c) M3 and (d) M4 at 0.3, 1, 5, 10, and 25 Myr. Topography below sea level is shown in shaded gray.

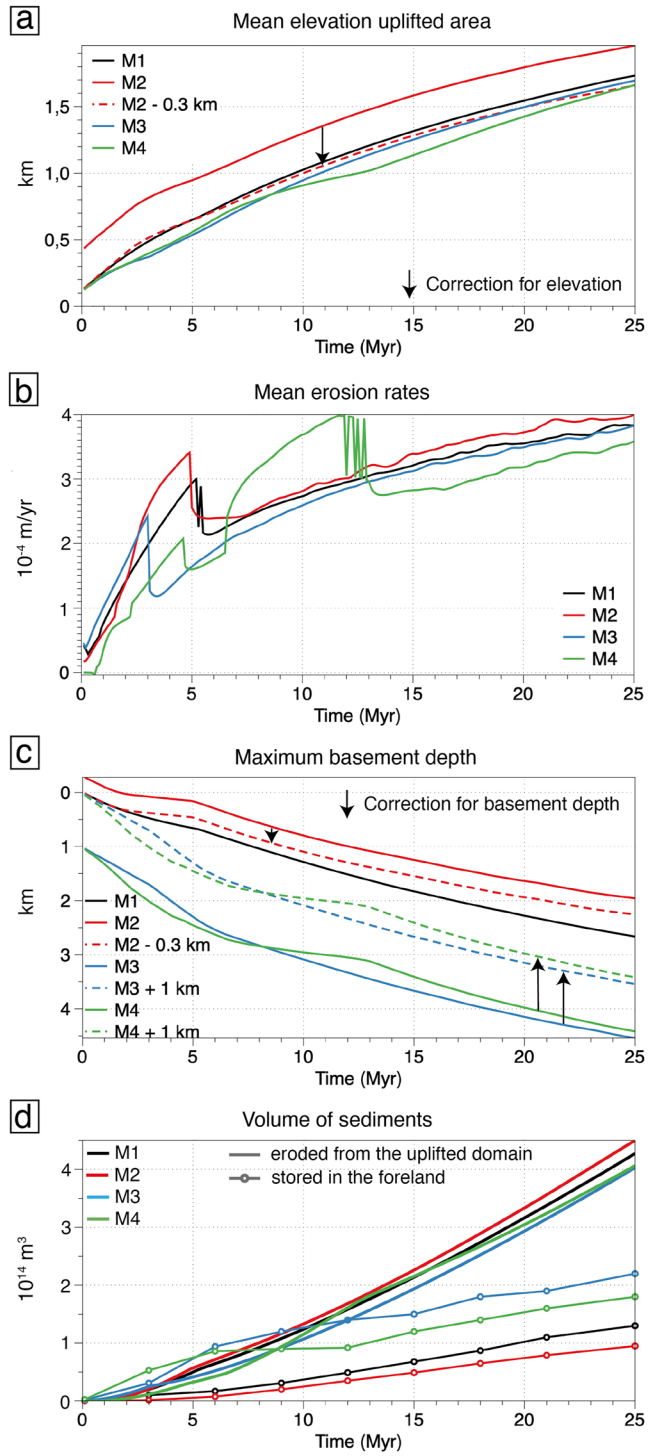

Figure 5. (a) Mean elevation of the uplifted domain of the four models through time. Dashed line for M2 is the elevation normalized to the other models, that is, corrected for additional topography (−300 m). (b) Mean erosion rates of the uplifted areas of the four models. (c) Maximum basement depth in the foreland of models (foredeep section, see location in Figure 1c). Dashed lines for M2–M4 are the basement depths normalized to model M1, that is, corrected for topography (−300 m) or additional bathymetry (+1,000 m). (d) Cumulative volumes of sediments produced in the mountain range (solid lines) and stored in the foreland basins (dotted lines). For models M3 and M4, volumes stored in the foreland basin are corrected from the volume of the initial bathymetry (40,000 km^3).

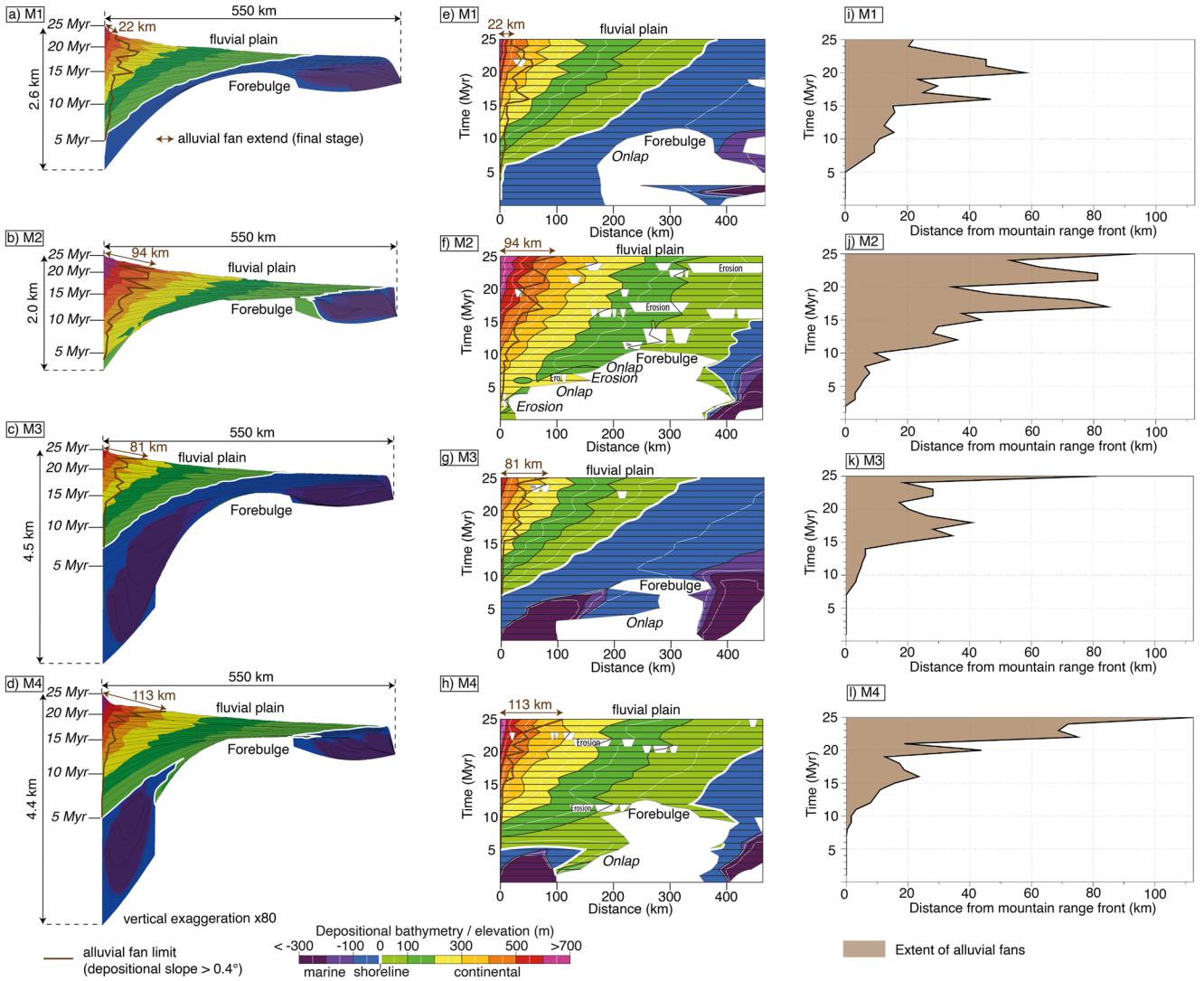

Figure 6. Stratigraphic architecture of the foreland basins of (a) M1, (b) M2, (c) M3 and (d) M4 models along the sections located in Figure 4. Sediments are colored according to their depositional bathymetry or elevation. Associated Wheeler diagrams of (e) M1, (f) M2, (g) M3, and (h) M4 models. The limit between fluvial plains and alluvial fans is extracted for portions, longer than 10 km, associated to depositional slopes >0.4° (Figure S5 in Supporting Information S1). Extent of alluvial fans in the foreland domain through time for (i) M1, (j) M2, (k) M3, and (l) M4.

in Figure 4). We highlight the transition from alluvial fan to fluvial plain deposits for sediments with a depositional slope >0.4° (Figure 6 and Figure S5 in Supporting Information S1; Bull, 1964; Milana & Ruzycki, 1999).

The foreland basin in reference model M1 has a maximum thickness of 2.6 km at the mountain front (Figure 6a). It shows continuous accumulation and is progressively filled up. Thus, it shows a shallowing trend, with shallow marine depositional environments at the base (water depth <100 m) evolving to continental depositional environments that record progressively increasing elevations (up to 500 m; Figures 6a and 6e). The shallow marine deposits of the foreland basin first onlap the forebulge before burying it by 12 Myr. Continental deposits are preserved at the foot of the mountain range from 5 Myr and progressively migrate (prograde) across the foreland domain to reach the open marine domain by 25 Myr. Alluvial fans propagate back and forth up to ~20 km within the foreland basin at 25 Myr (Figure 6i).

The foreland basin in model M2 is thinner than in reference model M1 (2 km) and includes only continental deposits (Figures 6b and 6f). It is filled by continental deposits at progressively higher elevation (up to 700 m). The continental sediments migrate across the foreland basin, onlap the forebulge and bury it by 11 Myr (i.e., slightly before model M1; Figures 6b and 6f). The continental foreland domain shows several local incisions, as

fluvial incision (channels of a few kilometers) or wider erosion areas (~80 km) develop, particularly above the buried forebulge, and remobilize previously deposited sediments. Alluvial fans propagate back and forth up to ~90 km within the foreland basin (Figure 6j).

The foreland basin in model M3 is ultimately significantly thicker than in reference model M1 (4.5 km) and includes deeper marine deposits (water depths >300 m; Figure 6c). As in model M1, it is progressively filled up in a shallowing trend, but from deep marine depositional environments at the base evolving to shallow marine and continental depositional environments that record progressively increasing elevations (up to 500 m; Figures 6c and 6g). The deep marine sediments progressively onlap the forebulge and shallow marine deposits bury it by 10 Myr (i.e., earlier than in model M1). Subsequently, similarly to model M1, the shoreline propagates across the foreland domain although alluvial fans propagate back and forth further within the foreland basin (up to ~80 km; Figure 6k).

The foreland basin in model M4 is as thick as in model M3 (4.4 km) and includes deep marine deposits as well (water depths >300 m; Figure 6d). As in model M3, it is progressively filled up in a shallowing trend, with deep marine depositional environments at the base evolving to shallow marine and continental deposits that however record ultimately higher elevations (>700 m; Figures 6d and 6h). As in model M1, the shoreline propagates across the foreland domain. However, the forebulge remains above sea level throughout the foreland basin infill, even feeding it with sediments resulting from its erosion. It is buried by continental deposits by 12 Myr. The continental foreland domain shows several local incisions, as fluvial incision develops and remobilizes previously deposited sediments. Alluvial fans propagate back and forth by more than 100 km in the foreland basin (Figure 6l).

3.5. Erosion and Accumulation Dynamics

Our models show specific erosion and sediment accumulation features. In reference model M1, erosion rates in the mountain range reduce sharply at 5.2 Myr and increase again steadily afterward (Figures 5b and 7). For M1, this drop of erosion rate is coeval with the coalescence of alluvial fans at the foot of the mountain range (Figures 7b and 8a). Models M2–M4 exhibit similar behavior with one or more drops in erosion rate that are also correlated to changes in depositional environments (transition from marine to continental fluvial plain deposits) or alluvial fan dynamics (transition from continental fluvial plain to alluvial fan deposits; Figure 5b, Figures S6–S8 in Supporting Information S1).

Figure 8 shows the co-evolution of depositional environments and bathymetry/elevation at the foot of the mountain range. In models M1, M3, and M4, transition from marine to continental depositional environments occurs between 3.0 and 4.6 Myr. In model M1, M2, and M3, alluvial fan build-up occurs between 4.9 and 6.0 Myr. Model M4 presents specific features in comparison to other models. Transition from marine to continental depositional environments corresponds to a first alluvial fan build-up (i.e., without preceding fluvial plain deposits) and a second phase of alluvial fan build-up occurs at 11.9 Myr (Figure 8d). The shoreline migration rates across the foreland are 23 and 17 km/Myr for M1 and M3, respectively (Figures 8a and 8c). For all models, the maximum elevation of the alluvial fan varies from 600 to 800 m at 25 Myr (Figure 8). It is higher for M2 and M4 (elevated foreland) than M1 and M3 (foreland at sea level). Interestingly, drops in erosion rates in the mountain range are coeval with the transition from marine to continental depositional environments or with alluvial fan coalescence in the foreland basin (Figures 5b, 7, and 8; Figures S6–S8 in Supporting Information S1).

4. Discussion

4.1. Stratigraphic Trends of the Foreland Domain Common to All Models

In terms of stratigraphic architecture, all models record a long-term prograding mega-sequence that is characteristic of foreland basin stratigraphic architectures (Figure 9a; e.g., DeCelles & Giles, 1996). During the initial stage of the simulation, the topographic load of the rising mountain range creates accommodation in the foreland basin by flexural isostasy and allows the storage of sediments at the foot of the mountain range. For a foreland domain initially at sea level (model M1), these sediments are initially deposited under shallow marine environments (Figure 9a). After 3.6 Myr, alluvial and alluvial fan deposits at the foot of the range (Figure 8a) mark the beginning of the prograding mega-sequence and of the transition of the foreland basin to the continentalization

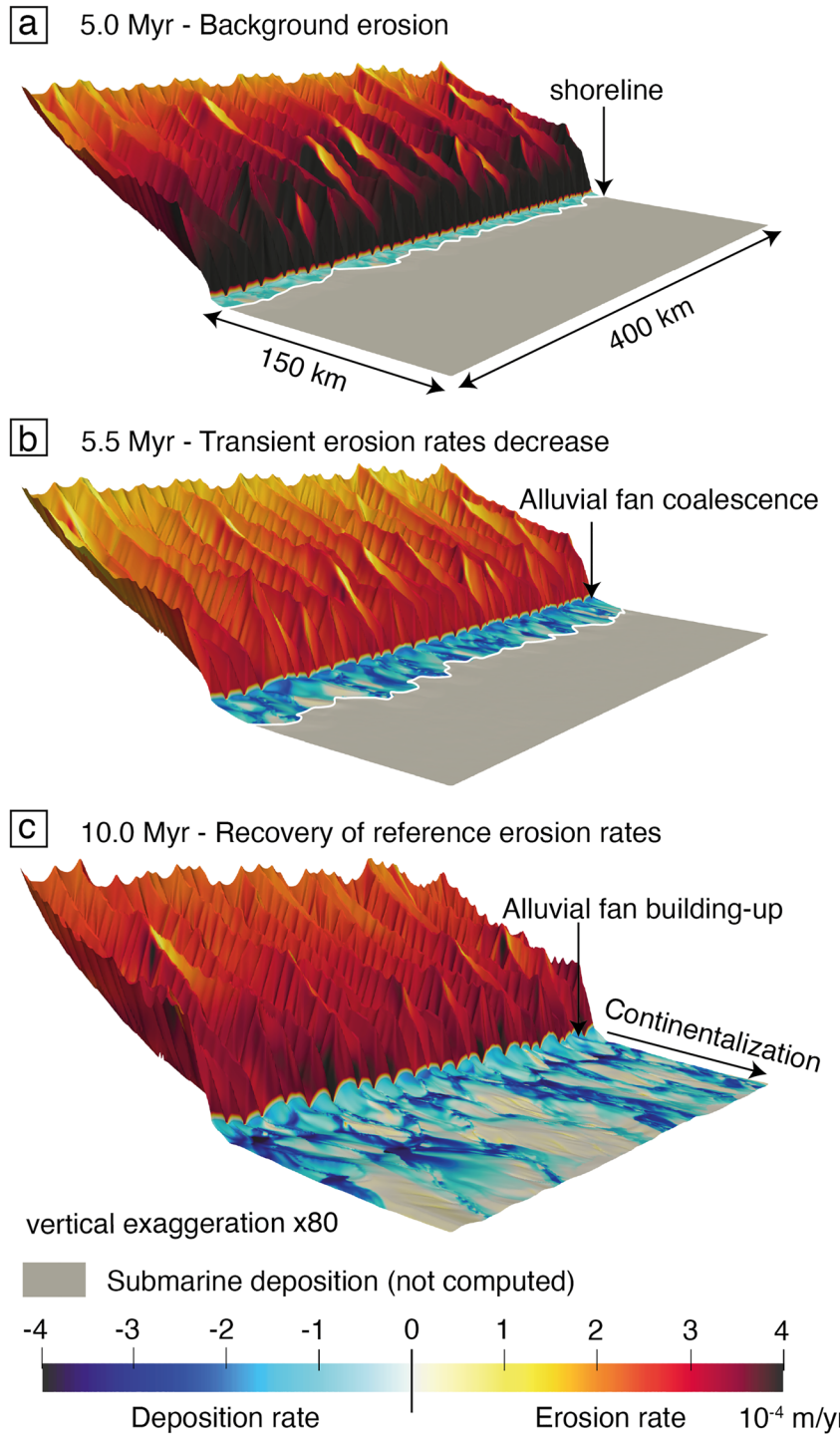

Figure 7. Zoom of the erosion and deposition rates of model M1 in the uplifted mountain range and proximal foreland domain at (a) 5 Myr (alluvial fan build-up initiation), (b) 5.5 Myr (alluvial fan coalescence), and (c) 10 Myr (after alluvial fan coalescence). Note the decrease in erosion rates in the uplifted area around 5.5 Myr. See location of the zoom area in Figure 4a.

phase. Then, the whole depositional profile (shoreline, alluvial, alluvial fans) migrates away from the mountain range recording the ongoing prograding (coarsening-up) mega-sequence (Figures 6 and 9). All models (M2–M4, SM1–SM4) display this long-term trend.

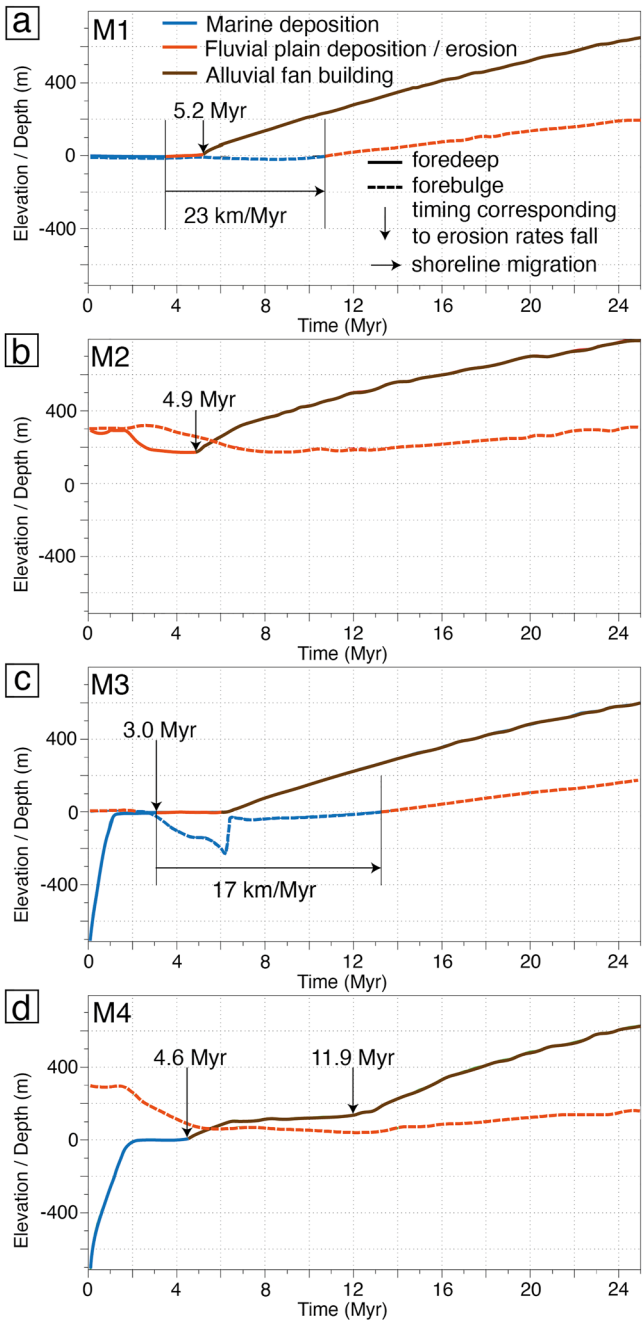

Figure 8. Evolution of depositional bathymetry/elevation of sediments at time of deposition along the foreland section (solid line) and forebulge section (dashed line; see location of sections in Figure 1c) for models M1–M4 (Figure 2). These curves represent the mean elevation values integrated along the sections (Figure 1c).

In all experiments, the sediment supply [S] produced by erosion of the uplifting mountain range is increasing over the 25 Myr of the simulation (Figure 5d). In parallel, the subsidence of the foreland basin basement is slowing down, hence reducing the accommodation space [A] creation in the foreland basin (Figure 5c). This reduction in accommodation space creation is driven by the slowing down of topographic loading over the time (Figure 5a). The drainage development in the mountain range and the associated erosion are progressively increasing in efficiency (as indicated by the volume of sediment produced; Figure 5d), reducing the rate of the mean topographic rise toward steady state (e.g., Babault et al., 2005; Carretier & Lucazeau, 2005; Tucker & van Der Beek, 2013), although it is not reached in 25 Myr of simulation (Figure 5a). As a result of these two coeval trends, the volume of sediments initially produced by erosion of the uplifting range is not sufficient to fill the space available for sedimentation. Then, progressively, the volume of sediments becomes equal and higher than the accommodation creation (overfilled phase). Although the proportion of sediments by-passing the foreland basin and exported to the open marine domain increases through time, the volume of sediment preserved in the foreland basin is increasing as well (Figure 5d) and drives the long-term prograding mega-sequence.

Another feature common to all models is that, once the foreland domain is fully continentalized (i.e., the long term progradation reaches the static forebulge), the sedimentary load is not limited to the foreland basin but is distributed over the entire accumulation area (foreland basin and forebulge; Figures 3, 6, and 9). Consequently, the impact of the sedimentary load in terms of differential subsidence/uplift between the foreland basin and the forebulge decreases after the continentalization and the burial of the forebulge (between 10 and 13 Myr in the models shown here). The accommodation in the foreland domain is then mostly controlled by the rise of the mountain and the distal marine base level. Over that period, the foreland basin progressively widens (Movies S1, S3, and S4). Leever et al. (2006) proposed that the migration of the orogenic load by the propagation of the thrust front away from the range could widen the flexural basin. We show here that, with a static orogenic load and thrust front, the sediment distribution can also induce a widening of the foreland basin even with a steady uplift of the range.

4.2. Influence of the Initial Elevation on the Stratigraphic Trend of the Foreland Domain

During the first 10 Myr, the landscape evolution of models M1–M4 is significantly different as a result of their inherited foreland domain bathymetry/topography (Figure 4). Interestingly, the influence of the initial relief largely disappears in the landscape of all models after ~10–13 Myr (Figure 4), after the foreland domain has been continentalized and its slope stabilized, that is, after the long-term prograding trend reaches the static forebulge. Afterward, all models show very similar landscape evolution with a continental foreland domain developing a transverse hydrographic network (Figure 4). Nevertheless, the initially different landscape evolution results in major differences in the stratigraphic architecture of the foreland basin.

First, the ultimate thickness of the foreland basin is very different. The foreland domain initially at sea level preserves up to 2.6 km of sediments, while the case with an elevated foreland domain preserves only 2 km and the case with an initially deep foreland domain preserves up to 4.5 km (Figures 6 and 9). As all models show a similar sediment production (Figure 5d), this difference results from the flexural response combined

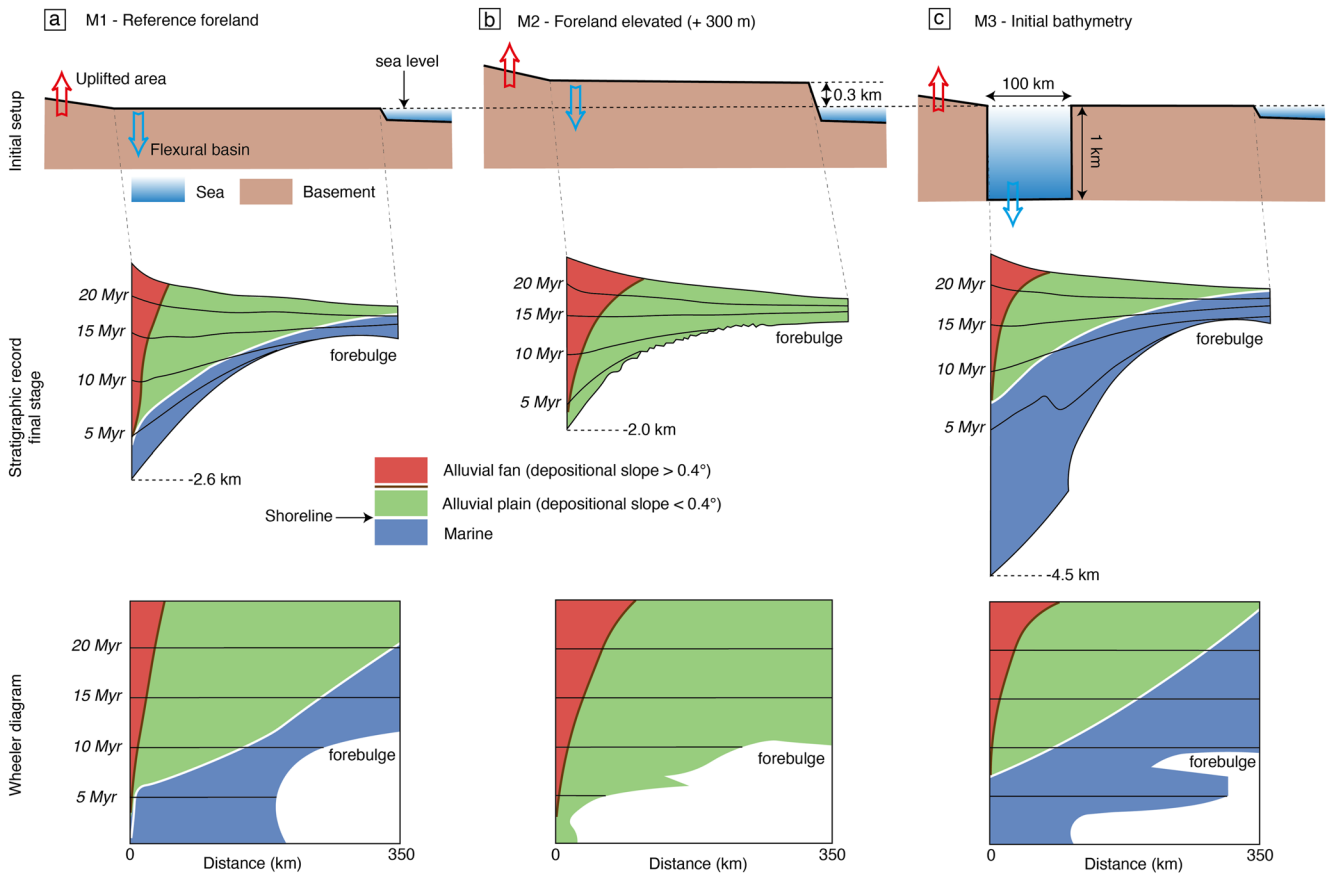

Figure 9. Schematic stratigraphic architecture for models (a) M1, (b) M2 and (c) M3. Upper panels show schematic cross-sections of the initial setups. Middle panels show schematic cross-sections of the depositional environments in the foreland basin. Bottom panels show associated schematic Wheeler diagrams.

with the initial capacity of the foreland domain to store sediments (directly controlled by its initial elevation). The additional load of the sediments trapped in the initial deep basin in the foreland domain (models M3 and M4) amplifies the flexural subsidence to create a thicker basin with respect to reference model M1 (Figures 5c and 5c). Conversely, the reduced sediment load in model M2 with an initially elevated foreland domain dampens the flexural subsidence and produces a thinner foreland basin with respect to model M1 (Figures 5a, 5c, and 5d). Flemings and Jordan (1989) have proposed that an increase in erosion or deposition efficiency, a higher EET or a slower thrust rate advance can result in a thicker foreland basin. We show here that an inherited bathymetry, such as a rift remnant, is another mechanism to produce a thicker foreland basin. Our models suggest that the deeper the initial rift remnant, the thicker the foreland basin deposits.

Second, the foreland domain initially at sea level preserves only 0.5 km of (shallow) marine sediments, while the elevated foreland domain preserves only continental deposits and the initially deep foreland domain up to 2.5 km of (deep) marine sediments (Figures 6 and 9). This is again the direct result of the foreland domain initial elevation impacting the depositional environments at which the long-term prograding mega-sequence initiates: deep marine, shallow marine, or continental. Our models show that, for the parameters used, an initially deep basin in the foreland domain is required to preserve a significant proportion of marine deposits in the foreland basin.

Third, a deep foreland also impacts the rate of progradation of the shoreline across the foreland domain. In the model with a deep inherited basin (M3), the continental deposits migrate more slowly (17 km/Myr) than in the model initially at sea level (M1; 23 km/Myr). In other words, the connection of the continental foreland domain to the open marine domain, (i.e., the main export of sediments to the open marine domain) is delayed by the infill of the initially deep inherited basin.

Fourth, the forebulge is buried under continental sediments in models with an initially elevated foreland (with or without a deep inherited basin; models M2 and M4) while it is buried by marine sediments in cases with a

foreland domain initially at sea level (with or without a deep inherited basin; models M1 and M3; Figures 6 and 9). The flexural subsidence in the foreland domain is sufficient to submerge the forebulge in experiments with a foreland domain at sea level but not in the experiment with an initially elevated foreland that remains above sea level throughout the experiment (Figures 4, 6 and 9). In addition, in an initially elevated foreland domain (with or without a deep inherited basin; models M2 and M4), continental and alluvial fan deposits reach ultimately higher elevations than in a foreland initially at sea level (with or without a deep inherited basin; models M1 and M3; Figures 6 and 9). Indeed, as the forebulge is acting as the base level once the foreland basin is filled up and continentalized, the more elevated the forebulge, the more elevated the upstream continental deposits (over 700 m for models M2 and M4 and about 500 m for models M1 and M3). The higher elevation of the alluvial fans also allows for their spreading further away from the mountain range (up to 111 km for model M2 and M4 and 40–80 km for models M1 and M2).

In summary, the occurrence of an inherited topography/bathymetry in the foreland domain does not alter the long-term prograding (shallowing-up) trend of the foreland basin. Indeed, for a constantly uplifting range, constant erodibility, for a given EET, the mean elevation of the range converges toward an equilibrium state and results in a coeval decrease in the rate of sediment production (Figure 5b) and of flexural accommodation space creation in the foreland basin. In all experiments, the decay in topographic building rates (Figure 5a) causes the attenuation of flexural subsidence in the foreland, which is in favor of the sediment volume that progressively fills up the accommodation volume and produces a prograding mega-sequence (Figure 9). Nonetheless, the decrease of the topographic building rates, associated with inherited topography bathymetry results in different rates of decay of sediment production in the range and accommodation creation in the foreland domain (Figure 5). This produces either deep marine, shallow marine or continental initial depositional environments in the foreland domain. It also impacts rates of progradation in the timing of the transition from marine to continental conditions. In an initially elevated foreland, the transition from marine to continental conditions occurs earlier and the progradation is faster than in initially deep foreland (Figure 9).

4.3. Feedback of the Foreland Domain Dynamics on Erosion Rates in the Mountain Range

We show above how inherited topography and/or bathymetry in the foreland domain impacts its subsidence and accumulation history. Our models also show that landscape dynamics in the foreland domain provide a feedback affecting the erosion dynamics of the mountain range. The abrupt drops in erosion rates in the uplifted domain (Figures 5b and 7) are synchronous with changes in the depositional systems at the foot of the mountain range. They systematically correspond to a transition from marine to continental depositional environments or from fluvial to alluvial fan deposits (Figures 7 and 8, Figures S6–S8 in Supporting Information S1). The continentalization of the foreland domain and the build-up and coalescence of alluvial fans, are associated with a raise of the base-level at the foot of the mountain range. Indeed, deposition at the orogenic piedmont will shift the elevation of the drainage basins upward since relief denudates at a lower rate than the uplift rate (Babault et al., 2005). This results in the increase of the absolute elevation of the topography by an amount equal to the mean elevation of the alluvial fan apex, which defines the base level of the uplifting relief (Babault et al., 2005). This base level rise is responsible for reducing the erosive potential for upstream areas and is thus responsible for the transient drops of erosion rates observed in the mountain range (Figures 5b and 7; Babault et al., 2005; Carretier & Lucazeau, 2005). After a while, the hydrographic network returns to its previous base level and erosion rates in the mountain range gradually return to similar but lower trends (Figure 5b). This autogenic feedback has previously been documented using both analog (Babault et al., 2005) and numerical modeling studies (Carretier & Lucazeau, 2005). This suggests that erosion rates in mountain ranges driven by climatic or tectonic forcing can also be modulated by downstream sedimentary dynamics. For example, the endorheic phase of the Ebro basin in the Eo-Oligo-Miocene (~37 and 16.5 Myr) resulted in substantial accumulation of continental deposits among others at high elevation at the foot of the southern Pyrenean range (e.g., Babault et al., 2005; Garcia-Castellanos et al., 2003). This period is characterized by a lowering in erosion rates in the mountain range that has been interpreted as resulting from the rise of the regional base-level (Babault et al., 2005; Garcia-Castellanos et al., 2003). The high-frequency oscillations in erosion rates observed in models M1 and M4 correspond to rapid coalescence and dispersal events of the alluvial fans at the foot of the range inducing transient rise and fall of the local base level (<500 kyr; e.g., Figure 5b). Indeed, the alluvial fans coalescence is not definitive as fans coalesce and disunite during a few time steps (Movies S1 and S4). However, these rapid oscillations do not impact the long-term erosion dynamics of the mountain range (Figure 5b).

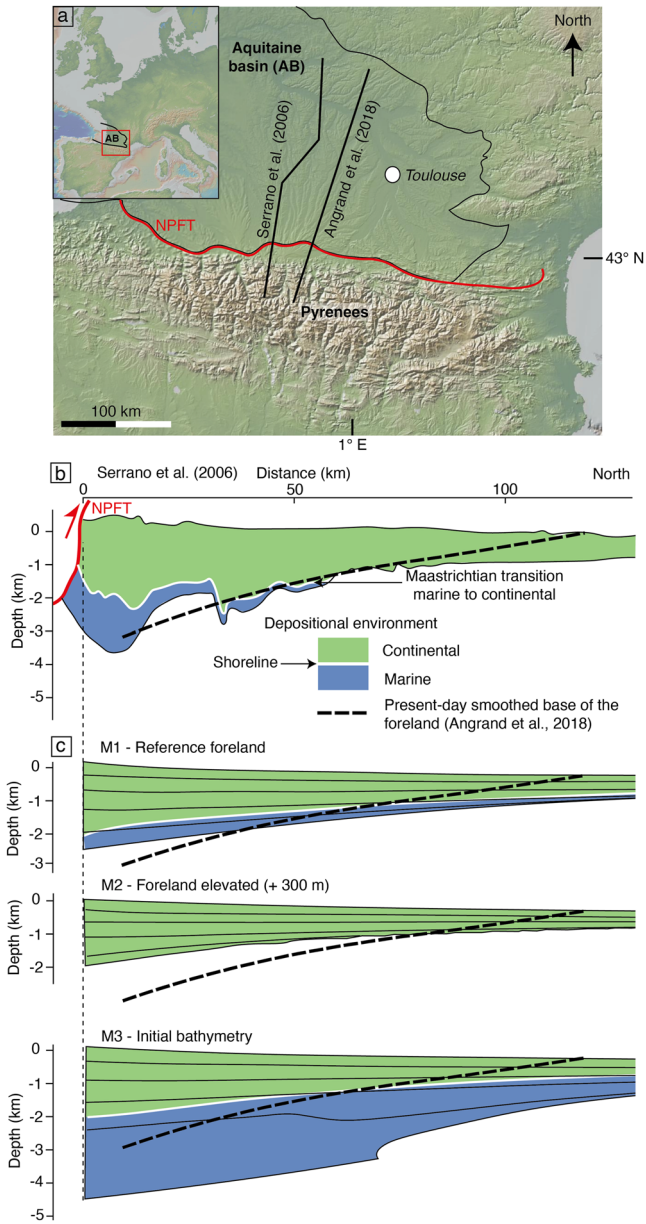

Figure 10. (a) Pyrenees and cross-section locations (from Angrand et al. (2018) and Serrano et al. (2006)). The inset shows Pyrenees and its associated Aquitaine retro-foreland basin location (red square) at the scale of Western Europe. (b) Cross-section of the Pyrenean retro-foreland stratigraphy (modified after Serrano et al., 2006). The transition from marine to continental depositional environment (Maastrichtian) is deduced from Rougier et al. (2016). Other marine deposits related to marine incursions later in the stratigraphic sequence (Ypresian) are not represented because of their limited thickness (<50 m; Rougier et al., 2016). (c) Cross-sections of foreland basin stratigraphic architectures and basement depth in models M1–M3. We plotted the present-day smoothed base of the Pyrenean retro-foreland from Angrand et al. (2018). AB: Aquitaine basin, outlined in black (Ortiz et al., 2020). NPFT: Northern Pyrenean Frontal Thrust.

4.4. Comparison With Natural Retro-Foreland Systems

We consider the implications of our model results for the northern retro-foreland system of the Pyrenees (Figure 10). The northern Pyrenees and the Aquitaine basin—Bay of Biscay system is a classic example of retro-wedge flexural foreland basin (Angrand et al., 2018; Bernard et al., 2019; Ortiz et al., 2020). Our set-up does not include several features of the Pyrenean system such as: horizontal displacement of thrusts, post-rift thermal subsidence (Angrand et al., 2018; Vacherat et al., 2014), basement heterogeneities in the retro-foreland basin (Angrand et al., 2018), geological and geometric complexities during mountain building (Vacherat et al., 2017), lateral variations in exhumation and uplift of the mountain range (Curry et al., 2021; Fillon & van der Beek, 2012; Fitzgerald et al., 1999), and the elbowed geometry of the North-Pyrenees—Aquitaine—Bay of Biscay system. Nevertheless, our simplified models exhibit first order features useful to understand the Pyrenean retro-foreland basins systems. The mean mountain range elevation after 25 Myr in the order of 1.5–2 km (Figure 5a) is consistent with the reconstructed mean elevation of the Pyrenean mountain range at the end of the syn-orogenic phase (e.g., Curry et al., 2019; Huyghe et al., 2012). The northern Pyrenean retro-foreland basin records a prograding mega-sequence similar to our models (e.g., Ford et al., 2016; Ortiz et al., 2020; Rougier et al., 2016). The Pyrenees developed by inversion of an inherited rifted domain (e.g., Desegaulx et al., 1991; Vacherat et al., 2017). The inherited pre-orogenic rift formed an initially deep foreland domain in the western sector of the Aquitaine foreland similar to models including an initial bathymetry at the foot of the range (M3 and M4). The maximum total subsidence at the thickest part of the Pyrenean retro-foreland (Central Pyrenees; close to ECORS line; Roure et al., 1989) ranges from 4 to 5 km-depth (Ford et al., 2016). These basement depths are consistent with our models including an initial bathymetry at the foot of the range (models M3 and M4; Figures 6 and 10) while it is shallower in models without (M1 and M2; Figures 6a, 10b, and 10c). The basement of the model M3 foreland basin is about 1 km deeper than in the Pyrenean case (Figure 10c), but its first-order stratigraphic architecture is consistent with the main trends of the present-day Pyrenean retro-foreland basin (Figures 10b and 10c). It shows deep initial depositional environments in the foreland basin similarly to the northern Pyrenean flysch, deposited in the late Cretaceous, during early convergence (Ford et al., 2016; Puigdefabregas & Souquet, 1986). It includes a significant section of marine sedimentary deposits like the one preserved in the Pyrenean retro-foreland basin (Serrano et al., 2006; Figure 10b). It also includes marine sedimentary deposits onlapping and burying the forebulge as in the Pyrenean retro-foreland basin (Serrano et al., 2006; Figure 10b). Our models show that an inherited bathymetry in the foreland basin associated with a forebulge area initially at sea level is critical to preserve sediments deposited in deep-marine depositional environments, to produce a thick marine sedimentary section in the retro-foreland, and to create a forebulge onlapped and buried by marine sediments (Figures 6c, 9, and 10). The configuration with a deep rift remnant in the foreland basin area and a low elevation of the forebulge area in model M3 is consistent with the paleogeographic reconstruction of Vacherat et al. (2017).

The northern Andean sediment routing system (~3,500 km for the Amazonian drainage area; Bajolet et al., 2022) is significantly longer than the northern Pyrenean one (~700 km) and the Andes has a significantly higher elevation. It is, however, interesting that the only regions in the Andean retro-foreland basin where marine, and especially deep marine, sediments are

preserved (e.g., Llanos basin (Colombia), Oriente basin (Ecuador), Ucayali basin (Peru)) correspond to former retro-arc basins (Horton, 2018). These retro-arc basins could have been associated to deep foreland areas like the one tested in M3 and M4. Regions located in between these basins, in the northern Andes area present a classical coarsening-up prograding sequence from shallow marine to continental deposits (Horton, 2018) more comparable to M1 (Figure 6a). In areas where the Andean foreland domain was initially elevated (outcropping basement of South American shields), the forebulge is mainly buried by continental sediments (Bajolet et al., 2022) as predicted by models M2 and M4 (Figure 6d).

In the Alpine retro-foreland, Paleogene to Miocene sedimentation in the basin is controlled by preserved Mesozoic extension related geometries (Turrini et al., 2016). Where initial accommodation space has been preserved from the rifting phase, the foreland basin is thicker preserving deep marine sediments (Turrini et al., 2016) as predicted by M3 and M4 (Figure 6c).

Our cylindrical set-up does not include several features of these natural retro-foreland systems (e.g., longitudinal drainage, horizontal displacement of thrusts, post-rift thermal subsidence, basement heterogeneities, lateral variations in exhumation and uplift of the mountain range, among others). However, it provides insight into the impact of several usually underestimated factors specifically the initial bathymetry and relief in the foreland domain that can provide an alternative explanation for some of the first order observations of the stratigraphic architecture of retro-foreland basins (thickness, preservation of deep marine deposits in the foreland basin and forebulge area, timing of the marine to continental transition).

4.5. Model Limitations

Thrust front propagation affects the syn-orogenic dynamics of foreland basins (Simpson, 2006), in particular by causing foreland migration of facies belts remobilizing previously deposited sediments at the foot of the mountain range as well as by inducing retrogradation phases in the foreland basin at the onset of thrusting events (Flemings & Jordan, 1990). The effects of thrust propagation are significant in pro-foreland systems where thrust front migration can exceed 100 km as for instance in the southern Pyrenean pro-wedge (Grool et al., 2018). Our models do not include horizontal deformation and cannot be used as an analog for pro-wedge systems. However, they are useful for understanding retro-foreland systems in which the maximum propagation of the deformation front is limited and less than 100 km. The northern Pyrenees are characterized by shortening of about 20 km (Grool et al., 2018). Naylor and Sinclair (2008) suggested that, in retro-foreland basins, the stratigraphic architecture is mostly controlled by the load of mountain range topography and the associated flexural isostatic subsidence of the foreland, whereas horizontal thrust propagation plays a subordinate role.

Natural examples of mountain range-foreland systems may also display lateral variations in the degree of shortening, amount of erosion, associated sediment delivery to the foreland or the location of the distal open marine domain. In the Pyrenees, basement depth varies from 1 to 3 km in the east to >5 km in the west. These variations have been mainly related to variations in extensional inheritance in the foreland (Angrand et al., 2018). The diachronous onset of the exhumation and topographic build-up from east to west (Vacherat et al., 2017) is also responsible for along strike variations in sediment supply which impact foreland basin filling and stratigraphic architecture (Michael et al., 2014; Ortiz et al., 2022; Verges, 2007). Our cylindrical modeling setup does not allow testing for these lateral variations, which may be investigated in future work using a non-cylindrical model setup. Nonetheless, Fastscape S2S does simulate in three dimensions depositional systems and lateral variations of deltas or alluvial fans at kilometric scale (Figure 4; Movies S1–S4). Note that these local sediment migrations along strike do not affect the long-term trends in sedimentary filling and stratigraphic architecture.

For sake of simplicity, in our models, global sea level, precipitation rate, uplift and sediment transport coefficient (K_f) are constant through time and homogenous in space. Furthermore, we do not include a multi-grain size distribution of the marine deposition and marine diffusion of sediments (e.g., sand vs. silt; Rouby et al., 2013; Yuan, Braun, Guerit, Simon, et al., 2019). Investigation of tectonic or climate-driven variations of sediment supply and the detailed stratigraphic architecture of the open-marine domain is, however, beyond the scope of our study as we focus on the long-term stratigraphic architecture of the foreland basin.

5. Conclusions

We investigate the influence of inherited foreland relief on the stratigraphic evolution of the foreland domain during the building of a mountain range using a LEM that couples continental and marine surface processes with

flexural isostasy. We show models with four different reliefs in the foreland domain: one initially at sea level, one initially at +300 m (continental foreland), one with a pre-existing 1 km-deep and 100 km-wide basin associated with either a forebulge area at sea level or elevated at +300 m.

Our models show that, during the first 10–13 Myr of model simulation, the landscape evolution of the foreland is significantly affected by inherited bathymetry/topography. However, the impact of the initial relief disappears in the landscape evolution once the foreland slope has stabilized and develops a transverse drainage network.

All models record a long-term prograding (coarsening-up and/or shallowing-up) trend of the foreland domain showing that, throughout the simulation, sediment production in the uplifting range is greater than the flexural creation of accommodation space in the foreland basin. Once the foreland domain is fully continentalized and the sedimentary load is distributed over the entire accumulation area (foreland basin and forebulge), the contribution of the differential subsidence between the foreland basin and the forebulge in the stratigraphic evolution decreases (after 10–13 Myr in the models shown here).

Models with different initial topography and/or bathymetry result in major differences in stratigraphic architectures of the foreland basin.

1. Initially deep basins lead to significantly thicker foreland deposits compared to a scenario with an initially elevated foreland.
2. An initially deep basin results in deposition and preservation of thick deep marine deposits while a foreland initially at sea level records only thin shallow marine deposits and the elevated foreland case only continental deposits.
3. The forebulge is buried under continental sediments in an initially elevated foreland (with or without a deep foreland basin) while it is buried by marine sediments in a foreland domain initially at sea level.
4. The elevation of alluvial fans at the foot of the range is higher (up to 200 m) in initially elevated foreland (with or without a deep foreland basin) than a foreland domain initially at sea level.
5. The initial topography and/or bathymetry of the foreland domain alters the timing of the transition from marine to continental phase: it occurs up to 5 Myr earlier in an initially elevated foreland compared with an initially deep foreland and the progradation rate is up to 35% faster.

All the models exhibit alluvial deposits and/or alluvial fan coalescence at the foot of the mountain belt that induces transient drops of erosion rates in the range by raising the local base level, showing how the dynamics of the depositional system at the foot of the mountain range may exert feedback on the erosion dynamics in the mountain range.

Comparison with the Pyrenean, Alpine and Andean retro-foreland basins shows that inherited bathymetry related to pre-orogenic rift structure, allows the deposition of a significant amount of syn-orogenic deep marine deposits and that a forebulge initially at sea level can be onlapped and buried under marine deposits. Although our cylindrical set-up does not include several features of these natural retro-forelands, it can provide usually underestimated factors related to the initial bathymetry and relief in the foreland domain to explain first order observations of the stratigraphic architecture of the retro-foreland basins (e.g., thickness, preservation of deep marine depositional environments in the foreland basin and forebulge area, timing of the marine to continental transition).

Data Availability Statement

We use in this study a Landscape Evolution Model (FastScape S2S; Yuan, Braun, Guerit, Rouby, & Cordonnier, 2019; Yuan, Braun, Guerit, Simon, et al., 2019; https://fastscape.org); The version of the program we use is the one published online on 26 April 2021 (release v0.1.0beta3; fastscapelib-fortran; public access) available on GitHub: https://github.com/fastscape-lem.

Acknowledgments
This work is part of the COLORS project, funded by TotalEnergies. We thank Fréderic Christophoul, Sebastian Wolf, Sébastien Carretier, and Josep Anton Muñoz for constructive discussions while writing the manuscript. We thank Mary Ford and an anonymous reviewer for constructive feedback on the manuscript.

References

Allen, P. A., Armitage, J. J., Carter, A., Duller, R. A., Michael, N. A., Sinclair, H. D., et al. (2013). The Qs problem: Sediment volumetric balance of proximal foreland basin systems. *Sedimentology*, *60*(1), 102–130. https://doi.org/10.1111/sed.12015

Angrand, P., Ford, M., & Watts, A. B. (2018). Lateral variations in foreland flexure of a rifted continental margin: The Aquitaine Basin (SW France). *Tectonics*, *37*(2), 430–449. https://doi.org/10.1002/2017TC004670

Armitage, J. J., Dunkley Jones, T., Duller, R. A., Whittaker, A. C., & Allen, P. A. (2013). Temporal buffering of climate-driven sediment flux cycles by transient catchment response. *Earth and Planetary Science Letters*, *369*(370), 200–210. https://doi.org/10.1016/j.epsl.2013.03.020

Babault, J., Bonnet, S., Crave, A., & Van Den Driessche, J. (2005). Influence of piedmont sedimentation on erosion dynamics of an uplifting landscape: An experimental approach. *Geology*, *33*(4), 301–304. https://doi.org/10.1130/G21095.1

Bajolet, F., Chardon, D., Rouby, D., Dall'Asta, M., Loparev, A., Couëffe, R., & Roig, J. Y. (2022). The sediment routing systems of Northern South America since 250 Ma. *Earth-Science Reviews*, *232*(February), 104139. https://doi.org/10.1016/j.earscirev.2022.104139

Beaumont, C. (1981). Foreland basins. *Geophysical Journal of the Royal Astronomical Society*, *65*(65), 291–329. https://doi.org/10.1111/j.1365-246x.1981.tb02715.x

Beaumont, C., Muñoz, J. A., Hamilton, J., & Fullsack, P. (2000). Factors controlling the Alpine evolution of the central Pyrenees inferred from a comparison of observations and geodynamical models. *Journal of Geophysical Research*, *105*(B4), 8121–8145. https://doi.org/10.1029/1999jb900390

Bernard, T., & Sinclair, H. D. (2022). Accelerated sediment delivery to continental margins during post-orogenic rebound of mountain ranges. *Basin Research*(September), 1–20. https://doi.org/10.1111/bre.12727

Bernard, T., Sinclair, H. D., Gailleton, B., Mudd, S. M., Ford, M., Recherches, C. D., et al. (2019). Lithological control on the post-orogenic topography and erosion history of the Pyrenees. *Earth and Planetary Science Letters*, *518*, 53–66. https://doi.org/10.1016/j.epsl.2019.04.034

Bovy, B. (2021). fastscape-lem/fastscape: Release v0.1.0beta3. https://doi.org/10.5281/ZENODO.4435110

Braun, J., & Willett, S. D. (2013). A very efficient O(n), implicit and parallel method to solve the stream power equation governing fluvial incision and landscape evolution. *Geomorphology*, *180–181*, 170–179. https://doi.org/10.1016/j.geomorph.2012.10.008

Bull, W. B. (1964). Geomorphology of segmented alluvial fans in western Fresno County, California. In *U.S. Geological Survey, Professional Paper, 352-E* (pp. 89–129).

Carretier, S., & Lucazeau, F. (2005). How does alluvial sedimentation at range fronts modify the erosional dynamics of mountain catchments? *Basin Research*, *17*(3), 361–381. https://doi.org/10.1111/j.1365-2117.2005.00270.x

Catuneanu, O. (2004). Retroarc foreland systems—Evolution through time. *Journal of African Earth Sciences*, *38*(7), 225–242. https://doi.org/10.1016/j.jafrearsci.2004.01.004

Catuneanu, O. (2017). *Sequence stratigraphy: Guidelines for a standard methodology* (Vol. 2). Elsevier. https://doi.org/10.1016/bs.sats.2017.07.003

Clevis, Q., de Boer, P. L., & Nijman, W. (2004). Differentiating the effect of episodic tectonism and eustatic sea-level fluctuations in foreland basins filled by alluvial fans and axial deltaic systems: Insights from a three-dimensional stratigraphic forward model. *Sedimentology*, *51*(4), 809–835. https://doi.org/10.1111/j.1365-3091.2004.00652.x

Curry, M. E., van der Beek, P., Huismans, R. S., Wolf, S. G., Fillon, C., & Muñoz, J. A. (2021). Spatio-temporal patterns of Pyrenean exhumation revealed by inverse thermo-kinematic modeling of a large thermochronologic data set. *Geology*, *49*(6), 738–742. https://doi.org/10.1130/G48687.1

Curry, M. E., van der Beek, P., Huismans, R. S., Wolf, S. G., & Muñoz, J. A. (2019). Evolving paleotopography and lithospheric flexure of the Pyrenean Orogen from 3D flexural modeling and basin analysis. *Earth and Planetary Science Letters*, *515*, 26–37. https://doi.org/10.1016/j.epsl.2019.03.009

Davy, P., & Lague, D. (2009). Fluvial erosion/transport equation of landscape evolution models revisited. *Journal of Geophysical Research*, *114*(3), 1–16. https://doi.org/10.1029/2008JF001146

DeCelles, P. G. (2012). Foreland basin systems revisited: Variations in response to tectonic settings. In B. P. Limited (Ed.), *Tectonics of sedimentary basins: Recent advances* (pp. 405–426). Blackwell.

DeCelles, P. G., & Giles, K. A. (1996). Foreland basin systems. *Basin Research*, *8*(2), 105–123. https://doi.org/10.1046/j.1365-2117.1996.01491.x

Densmore, A. L., Allen, P. A., & Simpson, G. (2007). Development and response of a coupled catchment fan system under changing tectonic and climatic forcing. *Journal of Geophysical Research*, *112*(1), 1–16. https://doi.org/10.1029/2006JF000474

Desegaulx, P., & Brunet, M.-F. (1990). Tectonic subsidence of the Aquitaine basin since Cretaceous times. *Bulletin de la Societe Geologique de France*, *8*(2), 295–306. https://doi.org/10.2113/gssgfbull.vi.2.295

Desegaulx, P., Kooi, H., & Cloetingh, S. (1991). Consequences of foreland basin development on thinned continental lithosphere: Application to the Aquitaine basin (SW France). *Earth and Planetary Science Letters*, *106*(1–4), 116–132. https://doi.org/10.1016/0012-821x(91)90067-r

Einsele, G. (1992). Basin classification and depositional environments (overview). *Sedimentary Basins*, 3–16. https://doi.org/10.1007/978-3-642-77055-5_1

Erdos, Z., Huismans, R. S., van der Beek, P., & Thieulot, C. (2014). Extensional inheritance and surface processes as controlling factors of mountain belt structure. *Journal of Geophysical Research: Solid Earth*, *119*(12), 9042–9061. https://doi.org/10.1002/2014JB011408.Received

Fillon, C., & van der Beek, P. (2012). Post-orogenic evolution of the southern Pyrenees: Constraints from inverse thermo-kinematic modelling of low-temperature thermochronology data. *Basin Research*, *24*(4), 418–436. https://doi.org/10.1111/j.1365-2117.2011.00533.x

Fitzgerald, P. G., Muñoz, J. A., Coney, P. J., & Baldwin, S. L. (1999). Asymmetric exhumation across the Pyrenean orogen: Implications for the tectonic evolution of a collisional orogen. *Earth and Planetary Science Letters*, *173*(3), 157–170. https://doi.org/10.1016/S0012-821X(99)00225-3

Flemings, P. B., & Jordan, T. E. (1989). A synthetic stratigraphic model of foreland basin development. *Journal of Geophysical Research*, *94*(B4), 3851–3866. https://doi.org/10.1029/jb094ib04p03851

Flemings, P. B., & Jordan, T. E. (1990). Stratigraphic modeling of foreland basins: Interpreting thrust deformation and lithosphere rheology. *Geology*, *18*(5), 430–434. https://doi.org/10.1130/0091-7613(1990)018<0430:SMOFBI>2.3.CO;2

Ford, M. K., Hemmer, L., Vacherat, A., Gallagher, K., & Christophoul, F. (2016). Retro-wedge foreland basin evolution along the ECORS line, eastern Pyrenees, France. *Journal of the Geological Society*, *173*(3), 419–437. https://doi.org/10.1144/jgs2015-129

Garcia-Castellanos, D., & Cloetingh, S. (2012). Modeling the interaction between lithospheric and surface processes in foreland basins. In C. Busby & A. Azor (Eds.), *Tectonics of sedimentary basins: Recent advances* (1st ed., pp. 152–181). Blackwell Publishing Ltd. https://doi.org/10.1002/9781444347166.ch8

Garcia-Castellanos, D., Vergés, J., Gaspar-Escribano, J., & Cloetingh, S. (2003). Interplay between tectonics, climate, and fluvial transport during the Cenozoic evolution of the Ebro Basin (NE Iberia). *Journal of Geophysical Research*, *108*(B7), 2347. https://doi.org/10.1029/2002jb002073

Grool, A. R., Ford, M., Vergés, J., Huismans, R. S., Christophoul, F., & Dielforder, A. (2018). Insights into the crustal-scale dynamics of a doubly vergent orogen from a quantitative analysis of its forelands: A case study of the Eastern Pyrenees. *Tectonics*, *37*(2), 450–476. https://doi.org/10.1002/2017TC004731

Guerit, L., Yuan, X. P., Carretier, S., Bonnet, S., Rohais, S., Braun, J., & Rouby, D. (2019). Fluvial landscape evolution controlled by the sediment deposition coefficient: Estimation from experimental and natural landscapes. *Geology*, *47*(9), 853–856. https://doi.org/10.1130/G46356.1

Horton, B. K. (2018). Sedimentary record of Andean mountain building. *Earth-Science Reviews*, *178*, 279–309. https://doi.org/10.1016/j.earscirev.2017.11.025

Huyghe, D., Mouthereau, F., & Emmanuel, L. (2012). Oxygen isotopes of marine mollusc shells record Eocene elevation change in the Pyrenees. *Earth and Planetary Science Letters*, *345–348*, 131–141. https://doi.org/10.1016/j.epsl.2012.06.035

Jordan, T. E. (1995). Retroarc foreland and related basins. *Tectonics of Sedimentary Basins*, 331–391.
Jordan, T. E., & Flemings, P. B. (1991). Large-scale stratigraphic architecture, eustatic variation, and unsteady tectonism: A theoretical evaluation. *Journal of Geophysical Research*, *96*(B4), 6681–6699. https://doi.org/10.1029/90jb01399
Leever, K. A., Bertotti, G., Zoetemeijer, R., Matenco, L., & Cloetingh, S. A. P. L. (2006). The effects of a lateral variation in lithospheric strength on foredeep evolution: Implications for the East Carpathian foredeep. *Tectonophysics*, *421*(3–4), 251–267. https://doi.org/10.1016/j.tecto.2006.04.020
Michael, N. A., Whittaker, A. C., Carter, A., & Allen, P. A. (2014). Volumetric budget and grain-size fractionation of a geological sediment routing system: Eocene Escanilla Formation, south-central Pyrenees. *Bulletin of the Geological Society of America*, *126*(3–4), 585–599. https://doi.org/10.1130/B30954.1
Milana, J. P., & Ruzycki, L. (1999). Alluvial-fan slope as a function of sediment transport efficiency. *Journal of Sedimentary Research*, *69*(3), 553–562. https://doi.org/10.2110/jsr.69.553
Naylor, M., & Sinclair, H. D. (2008). Pro-vs. retro-foreland basins. *Basin Research*, *20*(3), 285–303. https://doi.org/10.1111/j.1365-2117.2008.00366.x
Ortiz, A., Guillocheau, F., Lasseur, E., Briais, J., Robin, C., Serrano, O., & Fillon, C. (2020). Sediment routing system and sink preservation during the post-orogenic evolution of a retro-foreland basin: The case example of the North Pyrenean (Aquitaine, Bay of Biscay) Basins. *Marine and Petroleum Geology*, *112*(October 2019), 104085. https://doi.org/10.1016/j.marpetgeo.2019.104085
Ortiz, A., Guillocheau, F., Robin, C., Lasseur, E., Briais, J., & Fillon, C. (2022). Siliciclastic sediment volumes and rates of the North Pyrenean retro-foreland basin. *Basin Research*, *34*(March), 1–19. https://doi.org/10.1111/bre.12665
Puigdefabregas, C., & Souquet, P. (1986). Tecto-sedimentary cycles and depositional sequences of the mesozoic and tertiary from the Pyrenees. *Tectonophysics*, *129*(1–4), 173–203. https://doi.org/10.1016/0040-1951(86)90251-9
Quinlan, G. M., & Beaumont, C. (1984). Appalachian thrusting, lithospheric flexure, and the Paleozoic stratigraphy of the eastern interior of North America. *Canadian Journal of Earth Sciences*, *21*(9), 973–996. https://doi.org/10.1139/e84-103
Rouby, D., Braun, J., Robin, C., Dauteuil, O., & Deschamps, F. (2013). Long-term stratigraphic evolution of Atlantic-type passive margins: A numerical approach of interactions between surface processes, flexural isostasy and 3D thermal subsidence. *Tectonophysics*, *604*, 83–103. https://doi.org/10.1016/j.tecto.2013.02.003
Rougier, G., Ford, M., Christophoul, F., & Bader, A. G. (2016). Stratigraphic and tectonic studies in the central Aquitaine Basin, northern Pyrenees: Constraints on the subsidence and deformation history of a retro-foreland basin. *Comptes Rendus Geoscience*, *348*(3–4), 224–235. https://doi.org/10.1016/j.crte.2015.12.005
Roure, F., Choukroune, P., Berastegui, X., Munoz, J. A., Villien, A., Matheron, P., et al. (1989). ECORS deep seismic data and balanced cross sections: Geometric constraints on the evolution of the Pyrenees. *Tectonics*, *8*(1), 41–50. https://doi.org/10.1029/tc008i001p00041
Schlunegger, F., Jordan, T. E., & Klaper, E. (1997). Controls of erosional denudation in the orogen on foreland basin evolution: The Oligocene central Swiss Molasse Basin as an example. *Tectonics*, *16*(5), 823–840. https://doi.org/10.1029/97tc01657
Serrano, O., Delmas, J., Hanot, F., Vially, R., Herbin, J.-P., Houel, P., & Tourlière, B. (2006). Le Bassin d'Aquitaine: Valorisation des données sismiques, cartographie structurale et potentiel pétrolier. Edition BRGM, 245.
Simon, B., Robin, C., Rouby, D., Braun, J., & Guillocheau, F. (2022). Estimating sediment transport diffusion coefficients from reconstructed rifted margin architecture: Measurements in the Ogooué and Zambezi deltas. *Basin Research*, *34*(January), 2064–2084. https://doi.org/10.1111/bre.12696
Simpson, G. D. H. (2006). Modelling interactions between fold-thrust belt deformation, foreland flexure and surface mass transport. *Basin Research*, *18*(2), 125–143. https://doi.org/10.1111/j.1365-2117.2006.00287.x
Sinclair, H. D., & Allen, P. A. (1992). Vertical versus horizontal motions in the Alpine orogenic wedge: Stratigraphic response in the foreland basin. *Basin Research*, *4*(3–4), 215–232. https://doi.org/10.1111/j.1365-2117.1992.tb00046.x
Sinclair, H. D., Coakley, B. J., Allen, P. A., & Watts, A. B. (1991). Simulation of foreland basin stratigraphy using a diffusion model of mountain belt uplift and erosion: An example from Central Alps, Switzerland. *Tectonics*, *10*(3), 599–620. https://doi.org/10.1029/90tc02507
Stampfli, G. M., & Hochard, C. (2009). Plate tectonics of the Alpine realm. *Geological Society of London, Special Publications*, *327*(1), 89–111. https://doi.org/10.1144/sp327.6
Stewart, J., & Watts, A. B. (1997). Gravity anomalies and spatial variations of flexural rigidity at mountain ranges. *Journal of Geophysical Research*, *102*(B3), 5327–5352. https://doi.org/10.1029/96jb03664
Stock, J. D., & Montgomery, D. R. (1999). Geologic constraints on bedrock river incision using the stream power law. *Journal of Geophysical Research*, *104*(B3), 4983–4993. https://doi.org/10.1029/98jb02139
Theunissen, T., Huismans, R. S., Lu, G., & Riel, N. (2022). Relative continent—Mid-ocean ridge elevation: A reference case for isostasy in geodynamics. *Earth-Science Reviews*, *233*(January), 104153. https://doi.org/10.1016/j.earscirev.2022.104153
Tucker, G. E., & van der Beek, P. (2013). A model for post-orogenic development of a mountain range and its foreland. *Basin Research*, *25*(3), 241–259. https://doi.org/10.1111/j.1365-2117.2012.00559.x
Turrini, C., Toscani, G., Lacombe, O., & Roure, F. (2016). Influence of structural inheritance on foreland-foredeep system evolution: An example from the Po valley region (northern Italy). *Marine and Petroleum Geology*, *77*, 376–398. https://doi.org/10.1016/j.marpetgeo.2016.06.022
Vacherat, A., Mouthereau, F., Pik, R., Bernet, M., Gautheron, C., Masini, E., et al. (2014). Thermal imprint of rift-related processes in orogens as recorded in the Pyrenees. *Earth and Planetary Science Letters*, *408*, 296–306. https://doi.org/10.1016/j.epsl.2014.10.014
Vacherat, A., Mouthereau, F., Pik, R., Huyghe, D., Paquette, J. L., Christophoul, F., et al. (2017). Rift-to-collision sediment routing in the Pyrenees: A synthesis from sedimentological, geochronological and kinematic constraints. *Earth-Science Reviews*, *172*(July), 43–74. https://doi.org/10.1016/j.earscirev.2017.07.004
Verges, J. (2007). Drainage responses to oblique and lateral thrust ramps: A review. In G. Nichols, C. Paola, & E. Williams (Eds.), *Sedimentary processes, environments and basins: A Tribute to Peter Friend (IAS Special)* (pp. 29–47). Blackwell Publishing. https://doi.org/10.1002/9781444304411.ch3
Watts, A. B. (1992). The effective elastic thickness of the lithosphere and the evolution of foreland basins. *Basin Research*, *4*(3–4), 169–178. https://doi.org/10.1111/j.1365-2117.1992.tb00043.x
Whipple, K. X., & Tucker, G. E. (1999). Dynamics of the stream-power river incision model: Implications for height limits of mountain ranges, landscape response timescales, and research needs. *Journal of Geophysical Research*, *104*(B8), 661–674. https://doi.org/10.1029/1999jb900120
Willett, S., Beaumont, C., & Fullsack, P. (1993). Mechanical model for the tectonics of doubly vergent compressional orogens. *Geology*, *21*(4), 371–374. https://doi.org/10.1130/0091-7613(1993)021<0371:MMFTTO>2.3.CO;2
Wolf, S. G., Huismans, R. S., Muñoz, J. A., Curry, M. E., & van der Beek, P. (2021). Growth of collisional orogens from small and cold to large and hot—Inferences from geodynamic models. *Journal of Geophysical Research: Solid Earth*, *126*(2), 1–32. https://doi.org/10.1029/2020JB021168

Yuan, X. P., Braun, J., Guerit, L., Rouby, D., & Cordonnier, G. (2019). A new efficient method to solve the stream power law model taking into account sediment deposition. *Journal of Geophysical Research: Earth Surface*, *124*(6), 1346–1365. https://doi.org/10.1029/2018JF004867

Yuan, X. P., Braun, J., Guerit, L., Simon, B., Bovy, B., Rouby, D., et al. (2019). Linking continental erosion to marine sediment transport and deposition: A new implicit and O(N) method for inverse analysis. *Earth and Planetary Science Letters*, *524*, 1–15. https://doi.org/10.1016/j.epsl.2019.115728